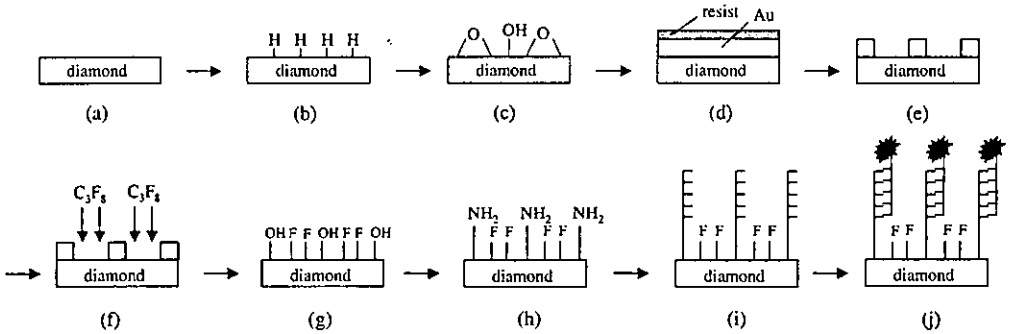

Fig. 1. Schematic representation of surface micropatterning DNA on single-crystal diamond by photolithography.

micropatterned areas were activated to generate a sufficient number of hydroxyl groups (Fig. 1(g)) and the amine moiety was then introduced using aminopropyltriethoxysilane (APTES) as described previously.[16] The amine-functionalized micropatterned surfaces were then used for micropatterning biomolecules (Fig. 1(h)).

To demonstrate the amine groups generated within the patterned regions and the fluorine termination outside the patterned regions, spatially resolved X-ray photoelectron spectroscopy (XPS) was used to characterize the chemical changes on the two different surfaces. However, due to the limitation of resolution in spatially resolved XPS, it is unable to characterize the amine-modified surface inside a 5 μm micropattern. Thus, larger micropatterns whose sizes are 500 μm were produced using the same photolithography fabrication process used for the 5 μm patterns. The amine-modified surface in the patterned area of 500 × 500 μm^2 and the fluorine-terminated layer between the patterns were then characterized by XPS with a Mg K_α X-ray (1253.6 eV) source. Figure 2 shows the XPS spectra of the two different APTES-modified and fluorine-terminated diamond surfaces. In the micropatterned regions modified with APTES, the main carbon and oxygen spectral peaks from bulk diamond were detected at 285.0 eV and 532.7 eV, respectively, corresponding to bulk carbon and oxygen. The Si (2p) spectrum shows a peak at 102.7 eV from the Si atom formed by a C-O-Si bond, revealing that APTES reacted with the hydroxylated surface. The N (1s) spectrum shows a significant peak centered at 400.6 eV, further showing that all of the nitrogen was present as amine. Another chemical functionalization of the diamond surface was accomplished by deprotecting trifluoroacetamide-protected 10-aminodec-1-ene (TFAAD)-modified diamond to generate amine groups on a polycrystalline diamond surface, in which the resulting amine groups show an N 1s peak at 401.0 eV and a C 1s peak at 285.5 eV.[10] These peaks are slightly different from the C 1s and N 1s peaks detailed above obtained by our method, mainly due to the chemical shift and our use of a different chemical modification method for producing amine groups on a single-crystal diamond surface. Additionally, the structure of an APTES film is complex, in that there are many possible conformations of the molecule and its orientation to the surface that can be realized. It appears that irreversible APTES multilayer formation or APTES polymerization takes place on a single-crystal diamond surface. In addition to the free primary amine groups, an

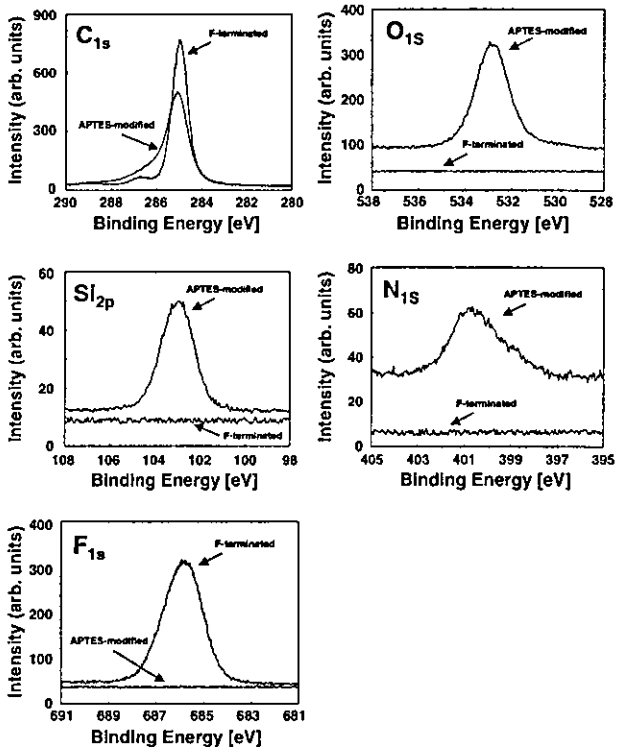

Fig. 2. X-ray photoelectron spectra of APTES-modified and fluorine-terminated diamond surfaces.

apparent shift might be expected for coordinated amine groups, resulting in an asymmetric N 1s peak. Nevertheless, at the surface terminated with fluorine, only C 1s and F 1s peaks were detected at 285.0 ev and 686.0 eV, respectively. However, no O 1s peak was observed on this surface. This result indicates that C_3F_8 plasma was successful in introducing fluorine termination outside micropatterned regions to form a passivation layer.

Subsequently, we covalently patterned amine-modified oligonucleotides on a single-crystal diamond surface using a crosslinker molecule, glutaraldehyde, as reported previously (Fig. 1(i)).[16] Two types of sequences, complementary and noncomplementary, were employed: H_2N-5′-CCACGGAC-TACTTCAAAACTA-3′ (complementary probe), H_2N-5′-ATCGATCGATCGATCGATCGA-3′ (noncomplementary probe). After patterning amine-modified DNA on diamond surfaces, the specificity of hybridization was explored by

using surface-immobilized sequences, both complementary and noncomplementary, to the applied fluorescently labeled DNA (Fig. 1(j)). The sequence of fluorescently labeled target oligonucleotides is Cy 5-5′-TAGTTTTGAAG-TAGTCCGTGG-3′ (target). The substrate was incubated with 1 μM Cy 5-labeled target oligonucleotides in 2 × SSC containing 0.2% Tween 20 (v/v) at 59°C for 2 h. The surface was then rinsed in a buffer and epifluorescence microscopy was performed to examine the specific hybridization process. Spatially well-ordered patterns of the hybridization of a target labeled with Cy 5 to the complementary probe were observed (Fig. 3(A)) with strong signals in the patterns and a low background outside the patterns, showing the strong specific binding of fluorescently labeled DNA to the complementary probes patterned on the diamond surface as expected. Fluorine termination on diamond has been reported.[17] However, to our knowledge, there has been no report that this termination can resist biomolecular adsorption. The fluorine-terminated surface between the patterns is hydrophobic, which was demonstated by a contact angle measurement (the contact angle is 110°C). Moreover, this surface is negatively charged by the electronegativity difference between carbon (2.5) and fluorine (4.0). Therefore, the fluorine termination is capable of minimizing the adsorption of DNA, which is also negatively charged, thereby significantly improving the signal-to-background ratio.

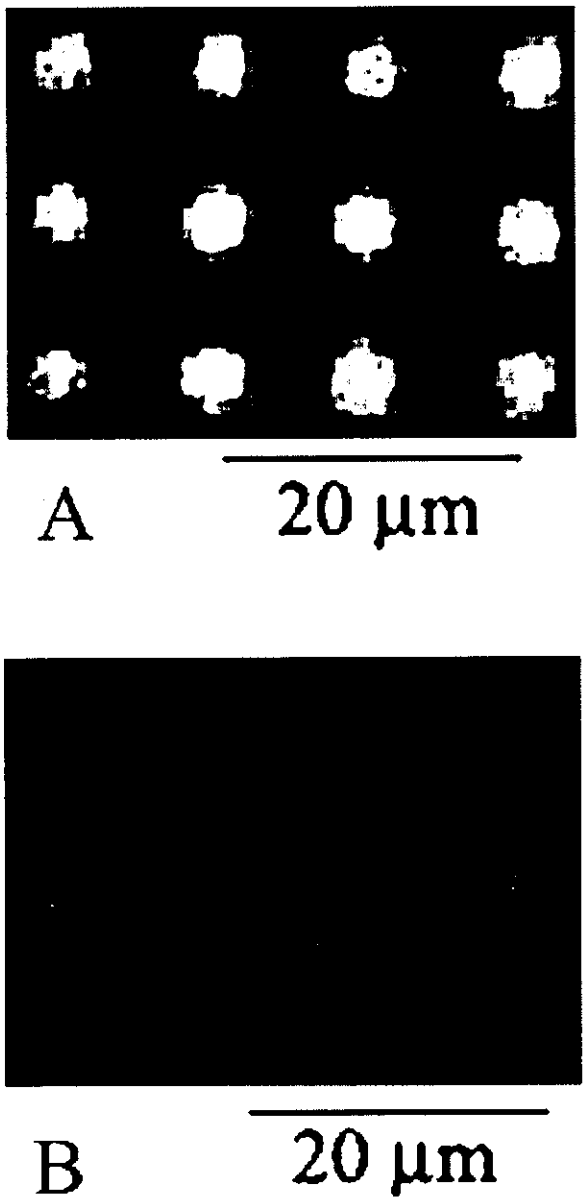

Fig. 3. Fluorescence micropatterns of hybridization of Cy 5-labeled DNA to two different probes complementary (A) and noncomplementary (B) patterned on single-crystal diamond surface. The size of each spot is 5 μm with center-to-center distance of 10 μm.

The unspecific binding of the noncomplementary probe with Cy 5-labeled target DNA was investigated using the same conditions as described above, resulting in a barely visible pattern (Fig. 3(B)). The control experiment indicates that no binding event occurs between the noncomplementary probe and the target duplex. These results demonstrate that both complementary and noncomplementary sequences are absolutely immobilized in a site-directed manner to the micropatterned areas on the surface and are accessible to hybridization. However, the subsequent hybridization only occurs at the complementary sequences.

In summary, micropatterning using a novel photolithographic process capable of introducing functionalized groups inside patterned regions and passivated termination outside patterned regions is demonstrated on a single-crystal diamond surface, and these chemically active micropatterns can be modified with biomolecules. The resulting patterns provide good control over the feature size and shape, the hydrophobic surface in the regions between the features, and the hydrophilic domain for the selective immobilization of biomolecules on micropatterns. The experiments detailed above show that the micropatterned DNA arrays exhibit extremely good selectivity for DNA attachment, high specificity for recognition, and high density for hybridization. Consequently, diamond is a unique material and has good biocompatibility that may enable superior support for biomolecular attachment. The combination of microelectronics fabrication with biological modification on diamond will benefit the development of integrated biosensors.

This work is supported in part by the Japan Society for the Promotion of Science (JSPS), the Core Research for Evolutional Science and Technology (CREST) of the Japan Science and Technology (JST) Corporation and a Grant-in-Aid for Center of Excellence (COE) Research from the Ministry of Education, Culture, Sports, Science and Technology.

1) F. Patolsky, A. Lichtenstein and I. Willner: J. Am. Chem. Soc. **123** (2001) 5194.
2) P. A. E. Piunno, U. J. Krull, R. H. E. Hudson, M. J. Damha and H. Cohen: Anal. Chim. Acta **288** (1994) 205.
3) R. A. Vijayendran and D. E. Leckband: Anal. Chem. **73** (2001) 471.
4) K. S. Song, T. Sakai, H. Kanazawa, Y. Araki, H. Umezawa, M. Tachiki and H. Kawarada: Biosens. Biolectron. **19** (2003) 137.
5) M. Milosevic, D. Sting and A. Rein: Spectroscopy **10** (1995) 44.
6) G. M. Swain and R. Ramesham: Anal. Chem. **65** (1993) 345.
7) H. J. Mathieu: Surf. Interface Anal. **32** (2001) 3.
8) L. Tang, C. Tasi, W. W. Gerberich, L. Kruckeberg and D. R. Kanie: Biomaterials **16** (1995) 483.
9) W. S. Yang, O. Auciello, J. E. Butler, W. Cai, J. A. Carlisle, J. E. Gerbi, D. M. Gruen, T. Knickerbocker, T. L. Lasseter, J. N. Russell,

J., L. M. Smith and R. J. Hamers: Nature Mater. **1** (2002) 253.
10) T. Knickerbocker, T. Strother, M. P. Schwartz, J. N. Russell, J., L. M. Smith and R. J. Hamers: Langmuir **19** (2003) 1938.
11) K. Ushizawa, Y. Sato, T. Mitsumori, T. Machinami, T. Ueda and T. Ando: Chem. Phys. Lett. **351** (2002) 105.
12) K. Takahashi, M. Tanga, O. Takai and H. Okamura: Diamond Relat. Mater. **12** (2003) 572.
13) T. Strother, T. Knickerbocker, J. N. Russell, J., J. E. Butler, L. M. Smith and R. J. Hamers: Langmuir **18** (2002) 968.
14) J. B. Miller and D. W. Brown: Langmuir **12** (1996) 5809.
15) H. Kanazawa, K. S. Song, T. Sakai, Y. Nakamura, H. Umezawa, M. Tachiki and H. Kawarada: Diamond Relat. Mater. **12** (2003) 618.
16) G.-J. Zhang, T. Tanii, T. Zako, T. Funatsu and I. Ohdomari: Sens. Actuat. B **97** (2004) 243.
17) J. S. Foord, N. K. Singh, R. B. Jackman, A. Gutierrez-Sosa, S. Proffitt and K. B. Holt: Surf. Sci. **488** (2001) 335.

Available online at www.sciencedirect.com
SCIENCE DIRECT®
Journal of Chromatography A, 1066 (2005) 41–45
JOURNAL OF CHROMATOGRAPHY A
www.elsevier.com/locate/chroma

High-performance liquid chromatographic assay of N^G-monomethyl-L-arginine, N^G,N^G-dimethyl-L-arginine, and N^G,$N^{G\prime}$-dimethyl-L-arginine using 4-fluoro-7-nitro-2,1,3-benzoxadiazole as a fluorescent reagent

Satoko Nonaka[a,1], Makoto Tsunoda[a,*,1], Kazuhiro Imai[b], Takashi Funatsu[a]

[a] *Graduate School of Pharmaceutical Sciences, The University of Tokyo, 7-3-1 Hongo, Bunkyo-ku, Tokyo 113-0033, Japan*
[b] *Research Institute of Pharmaceutical Sciences, Musashino University, 1-1-20 Shinmachi, Nishitokyo-shi, Tokyo 202-8585, Japan*

Received 2 November 2004; received in revised form 11 January 2005; accepted 21 January 2005

Abstract

N^G-Monomethyl-L-arginine (L-NMMA), N^G,N^G-dimethyl-L-arginine (ADMA), and N^G,$N^{G\prime}$-dimethyl-L-arginine (SDMA) are emerging cardiovascular risk factors. A high-performance liquid chromatographic method with fluorescence detection for the simultaneous determination of L-NMMA, ADMA and SDMA is described. The assay employed 4-fluoro-7-nitro-2,1,3-benzoxadiazole (NBD-F) as a fluorescent derivatization reagent. After solid phase extraction with cation-exchange column, the methylated arginines were converted to fluorescent derivatives with NBD-F, and the derivatives were separated within 32 min on a reversed-phase column. N^{ω}-Propyl-L-arginine was used as an internal standard. Extrapolated detection limits were 12 nM (12 fmol per injection) for L-NMMA and 20 nM (20 fmol per injection) for ADMA and SDMA, respectively, with a signal-to-noise ratio of 3. The calibration curves for L-NMMA, ADMA and SDMA were linear within the range of 50–5000 fmol. The method was applied to the quantitative determination of L-NMMA, ADMA and SDMA in 200 μl of rat plasma. The concentrations of L-NMMA, ADMA and SDMA in rat plasma were 0.16 ± 0.03, 0.80 ± 0.25 and 0.40 ± 0.21 μM, respectively ($n = 5$).

Keywords: N^G,N^G-Dimethyl-L-arginine (ADMA); Nitric oxide synthase; 4-Fluoro-7-nitro-2,1,3-benzoxadiazole; Fluorescence

1. Introduction

Nitric oxide (NO), synthesized from L-arginine by nitric oxide synthase (NOS), plays important roles in the regulation of blood flow and blood pressure, inhibition of platelet aggregation, and neurotransmission [1]. N^G-Monomethyl-L-arginine (L-NMMA), N^G,N^G-dimethyl-L-arginine (ADMA), and N^G,$N^{G\prime}$-dimethyl-L-arginine (SDMA) (Fig. 1) are formed from the degradation of methylated proteins [2]. Asymmetrical methylarginines, L-NMMA and ADMA, presented in plasma are inhibitors for NOS [3,4]. Though SDMA has no biological activity like L-NMMA and ADMA, it can interrupt the transportation of cationic amino acids such as L-arginine into cell [5]. Thus, high concentrations of SDMA in plasma may reduce NO production [6].

Increased concentration of methylated arginines in plasma is associated with hypertension [7], renal failure [8], hypercholesterolemia [9], and diabetes mellitus [10]. Furthermore, previous data on the impairment of arginine metabolism or pools in spontaneously hypertensive rats prompted us to investigate the involvement of the methylated arginines in the hypertensive rats [11,12]. Therefore, measurements of the concentration of these methylated arginines are important for the study of the arginine–NO system and endogenous inhibitors for NOS. However, a reliable and highly sensitive analytical method is lacking.

* Corresponding author. Tel.: +81 3 5841 4761.
E-mail address: makotot@mol.f.u-tokyo.ac.jp (M. Tsunoda).
[1] These authors contributed equally to this work.

0021-9673/$ – see front matter © 2005 Elsevier B.V. All rights reserved.
doi:10.1016/j.chroma.2005.01.052

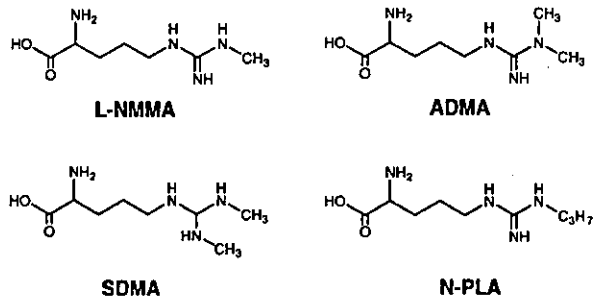

Fig. 1. Chemical structures of methylated arginines (L-NMMA, ADMA, SDMA and N-PLA).

Analytical methods for the determination of methylated arginines include thin layer chromatography [13], electrophoresis [14], ion exchange chromatography [15,16], and monoclonal antibody assay [17]. Recently, liquid chromatography–mass spectrometry (LC–MS) [18,19] and capillary electrophoresis with laser-induced fluorescence (CE-LIF) detection [20] have been the most sensitive determination methods. However, these methods are not ideal for routine clinical purposes because the procedures are time-consuming and the instrumentation is not always available in a routine clinical laboratory.

Reversed-phase high-performance liquid chromatography (HPLC) has also been employed for the sensitive analysis of methylated arginines. These methods include fluorescence detection, and *o*-phthalaldehyde (OPA) was the most commonly used fluorescent derivatization reagent [21–25]. However, OPA derivatives are unstable. Besides the loss of fluorescence during HPLC analysis, methylated arginines were not well resolved under certain chromatographic conditions [21–23,25]. Furthermore, because the concentration of L-NMMA is lower than that of ADMA and SDMA, fluorescence intensities of OPA derivatives were not efficient to determine three methylated arginines simultaneously. 4-Fluoro-7-nitro-2,1,3-benzoxadiazole (NBD-F) was developed as a fluorescent derivatization reagent for amino acid [26]. This reagent has much higher sensitivity and stability than OPA. The purpose of our study was the development of a new method for the simultaneous and sensitive analysis of three methylated arginines using NBD-F as a fluorescent derivatizing reagent.

2. Experimental

2.1. Materials

L-NMMA, ADMA and SDMA were obtained from Sigma (St. Louis, MO, USA). A stock standard solution was stored in 10 mM HCl at 4 °C. N^{ω}-Propyl-L-arginine (N-PLA, Fig. 1) was obtained from Calbiochem (San Diego, CA, USA). NBD-F and boric acid were purchased from Wako (Osaka, Japan). Acetonitrile and methanol (HPLC grade) were obtained from Kanto Kagaku (Tokyo, Japan). Oasis MCX cation-exchange SPE columns (1 ml) were supplied by Waters (Milford, MA, USA). Water was used after purification by a Milli-Q reagent system (Nihon Millipore, Tokyo, Japan).

2.2. Biological samples

Male Sprague–Dawley (SD) rats (8 weeks old) were purchased from Charles River Japan (Kanagawa, Japan). The blood samples were collected into heparinized polyethylene tubes, and were immediately centrifuged at $1710 \times g$ for 10 min at 4 °C. The plasma fraction was collected and stored at −80 °C until the analysis.

2.3. Extraction procedure

L-NMMA, ADMA and SDMA were extracted from plasma samples with Oasis MCX cation-exchange SPE columns at room temperature. The SPE columns were used without preconditioning, and all washing and elution steps were performed by vacuum suction. A Vac-Elut sample preparation manifold, with a capacity of 10 columns (Varian, Harbor City, CA, USA) was used for the SPE procedure. Oil-sealed rotary vacuum pumps GLD-131 C (Ulvac Kiko, Yokohama, Japan) and centrifugal concentrator VC-36N (Taitec, Saitama, Japan) were used for evaporation procedure.

Before analysis, 200 μl of plasma or standard solution was mixed with 100 μl of N-PLA solution and then diluted by adding 700 μl of 50 mM borate buffer (pH 9.0). The solution was applied on the column. The columns were consecutively washed with 1.0 ml of 50 mM borate buffer (pH 9.0), 3.0 ml of water and 1.0 ml of methanol. Methylated arginines were eluted into 2.0 ml tubes with 1.0 ml of concentrated ammonia–water–methanol (10:40:50, v/v/v). The solvent was then evaporated to dryness at 60 °C. The dried extract was dissolved in 100 μl of water and used for the derivatization.

2.4. Derivatization procedure

First, 105 μl of 100 mM borate buffer (pH 9.0) and 30 μl of 40 mM NBD-F in acetonitrile were added to the 30 μl of sample. Then, the reaction was incubated at 40 °C for 3 min. To stop the reaction, 435 μl of 0.5% acetic acid (v/v) was added. A 10 μl aliquot of sample was injected onto the HPLC.

2.5. Chromatographic conditions

The chromatographic system was composed of Pump L-7100 (Hitachi, Tokyo, Japan), 655A-52 Column Oven (Hitachi) and FP-920S intelligent fluorescence detector (Jasco, Tokyo, Japan). The column used was Unison UK-C_{18} (150 mm × 4.6 mm I.D., Imtakt, Kyoto, Japan).

Mobile phase A consisted of 50 mM sodium phosphate buffer (pH 3.2)–acetonitrile (91:9, v/v), and mobile phase B was acetonitrile. The gradient program was as follows; 0–18 min 100% A, 18–28 min linear change to 70% A,

28–32 min 70% A. The flow rate was set at 0.75 ml/min, and the column oven was maintained at 40 °C. The wavelengths of the fluorescence detector were set at 470 and 530 nm for excitation and emission, respectively.

2.6. Examination of stability of the NBD-F derivatives

Standard solution containing 10 μM L-NMMA, ADMA, SDMA and N-PLA was reacted with NBD-F under the condition expressed above. Stability of the NBD-F derivatives at room temperature was examined for 3 days.

2.7. Validation

Calibration standards for L-NMMA, ADMA and SDMA (1, 2, 5, 10, 20, 50 and 100 μM) were prepared from stock solutions. Additional calibration curves were performed by mixing 200 μl plasma, 100 μl standard solution, 100 μl of 40 μM N-PLA solution and 600 μl of 50 mM borate buffer (pH 9.0). Concentrations of standard samples were 0.5, 1.0, and 2.0 μM. Calibration curves were calculated by plotting the peak area ratios of analyte over internal standard versus analyte concentration.

The intra-day assay precision was determined by five replicate analyses of the plasma samples on the same day, while the recovery was evaluated simultaneously. The inter-day assay precision was determined by analyzing one sample on five different days.

Plasma data were presented as mean ± standard deviation.

3. Results and discussion

3.1. Fluorescent derivatization of methylated arginines with NBD-F

In order to increase the efficiency of derivatization, some parameters such as pH, temperature and reaction time were examined.

It was reported that the optimum pH for the derivatization of amines with NBD-F was above 8 [26]. Therefore, the pH of the derivatization reaction was investigated ranged from 8.0 to 9.0. As shown in Fig. 2, at pH 9.0, the maximum fluorescence intensity was obtained among the pH ranged examined.

Then, optimum temperature was studied, ranged from 40 to 60 °C. Each fluorescence intensity was similar. Because there was less by-products on the chromatogram at 40 °C as compared with 60 °C (data not shown), 40 °C was selected as the optimum temperature. Finally, the optimum fluorescent derivatization condition for 3 min at 40 °C at pH 9.0 was chosen.

3.2. Separation of L-NMMA, ADMA and SDMA

First, the separation of L-NMMA, ADMA and SDMA was investigated under isocratic condition using the mobile phase consisted of 50 mM sodium phosphate buffer (pH 3.2)–acetonitrile (91:9, v/v). However, under the isocratic condition, SDMA was not separated from a by-product. The derivatized samples were then separated on an ODS column using a gradient elution system, and SDMA and the by-product could be separated from each other. The optimum gradient program is described in Section 2.5 above. Fig. 3 illustrates the typical chromatograms of (A) standard solution and (B) rat plasma sample. L-NMMA, ADMA and SDMA were well separated within 32 min.

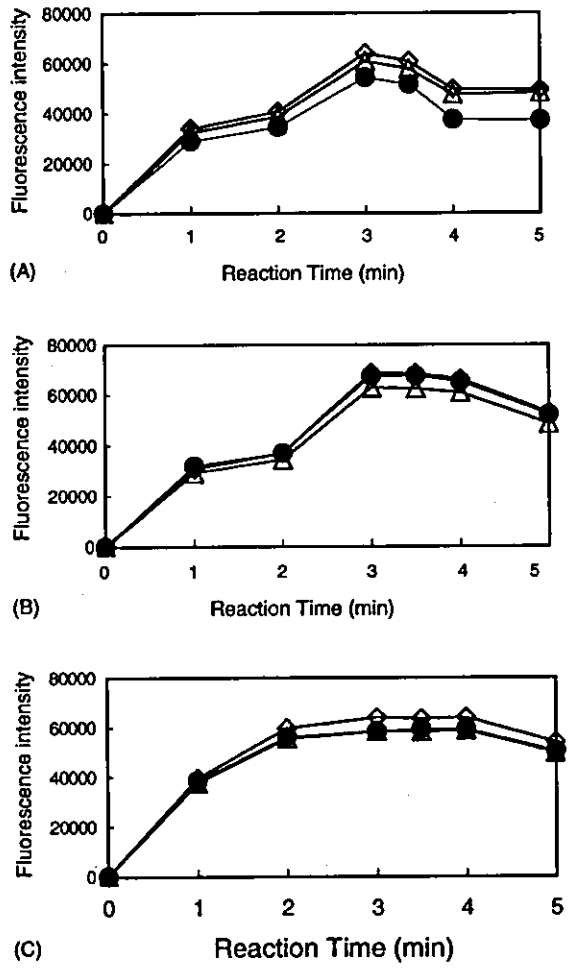

Fig. 2. Effect of pH and reaction time of fluorescent derivatization on the fluorescence intensities of NBD–L-NMMA (◇), NBD–ADMA (△) and NBD–SDMA (●): (A) pH 8.0; (B) pH 8.5; and (C) pH 9.0. The precisions for each point were less than 2%.

3.3. Linearity, detection limit, precision and accuracy

Using the method described here, a validation study on the methylated arginines in rat plasma samples was carried out. Linearity was assessed by adding known amounts of L-NMMA, ADMA and SDMA to rat plasma such that the concentrations ranged from 0.5 to 2 μM. The results were $r^2 > 0.99$ each. Limits of detection (LOD) for the method were

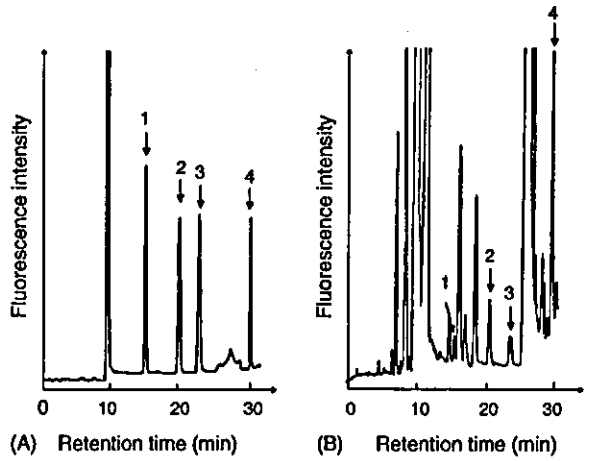

Fig. 3. (A) Chromatogram of a standard mixture containing (1) 10 μM L-NMMA; (2) 10 μM ADMA; (3) 10 μM SDMA; and (4) 5.0 μM N-PLA as internal standard. (B) Chromatogram of rat plasma sample (200 μl) containing (1) 0.17 μM L-NMMA; (2) 0.63 μM ADMA; (3) 0.30 μM SDMA; and (4) 1.5 μM N-PLA as internal standard. A 10 μl aliquot of sample from reaction mixture (600 μl) was injected onto the HPLC. Other HPLC conditions are described in Section 2.

12 fmol for L-NMMA, and 20 fmol for ADMA and SDMA at signal-to-noise ratio of 3 with standard samples, while the LODs for ADMA and SDMA using OPA derivatization and fluorescence detection were reported to be 50–200 fmol [21–23,25].

Intra-day assay CVs ($n=5$) for L-NMMA, ADMA and SDMA were 2.89, 5.56 and 2.44%, respectively. Inter-day assay CVs ($n=5$) for L-NMMA, ADMA and SDMA were 9.50, 6.73 and 8.58%, respectively. Data on accuracy, expressed as recovery of analyte from spiked plasma samples ($n=3$), are depicted in Table 1. These data showed good reproducibility of the present HPLC method.

Table 1
Accuracy and precision data for determination of L-NMMA, ADMA and SDMA

	Concentration (mean ± SD, μM)	Precision (RSD, %)	Recovery (%)
L-NMMA added, μM ($n=3$)			
0	0.17 ± 0.005	2.89	
0.5	0.68 ± 0.004	0.58	102
1.0	1.2 ± 0.006	0.52	99
2.0	2.2 ± 0.008	0.37	101
ADMA added, μM ($n=3$)			
0	0.72 ± 0.04	5.56	
0.5	1.2 ± 0.04	3.25	102
1.0	1.7 ± 0.06	3.51	99
2.0	2.8 ± 0.09	3.19	105
SDMA added, μM ($n=3$)			
0	0.41 ± 0.01	2.44	
0.5	0.90 ± 0.03	3.33	98
1.0	1.4 ± 0.05	3.60	98
2.0	2.4 ± 0.06	2.47	101

3.4. Stability of the NBD-F derivatives

In previous reports [21,23], OPA derivatives were found to be unstable, which may lead to a loss in precision and accuracy of the assay. Marra et al. found that naphthalene–2,3-dicarboxaldhyde (NDA) derivatives were more stable than the OPA derivatives [27]. In this study, we focused on the improvement of the stability of derivatives by using NBD-F as fluorescent derivatizing reagent.

Each fluorescence of the NBD-F derivatives of standards (L-NMMA, ADMA, SDMA and N-PLA) was stable for at least 3 days at room temperature. This data clearly demonstrate that our method has much better stability of fluorescence derivatives over time compared to the previous methods. Thus, a large number of samples could be derivatized in one time, and stored at room temperature for at least 3 days before analysis.

3.5. Concentration of L-NMMA, ADMA and SDMA in rat plasma

The concentrations of L-NMMA, ADMA and SDMA in rat plasma were 0.16 ± 0.03, 0.80 ± 0.25 and 0.40 ± 0.21 μM, respectively ($n=5$). The mean rat plasma levels of methylated arginines were in agreement with an earlier report (0.18, 0.60 and 0.30 μM for L-NMMA, ADMA and SDMA, respectively) [24].

4. Conclusions

A method for the simultaneous determination of L-NMMA, ADMA and SDMA was developed using NBD-F as a fluorescent derivatization reagent. Fluorescent derivatives of methylated arginines with NBD-F were highly sensitive and stable compared with other fluorescent derivatives. The method may be useful in the investigation of the role of methylated arginines in a large number of pathological conditions.

Acknowledgements

The authors thank Dr. Chang-Kee Lim, MRC Bioanalytical Science Group, for his kind suggestions and valuable discussion. We would like to thank Imtakt for his kind supply of Unison UK-C_{18} column. This research was supported in part by grants (to M.T.) from the Mitsubishi Chemical Corporation Fund and from Takeda Science Foundation.

References

[1] S. Moncada, A. Higgs, N. Engl. J. Med. 329 (1993) 2002.
[2] J.R. McDermott, Biochem. J. 154 (1976) 179.
[3] P. Vallance, A. Leone, A. Calver, J. Collier, S. Moncada, J. Cardiovasc. Pharmacol. 20 (1992) 60.

[4] J. Leiper, P. Vallance, Cardiovasc. Res. 43 (1999) 542.
[5] E.I. Closs, F.Z. Basha, A. Habermeier, U. Forstermann, Nitric Oxide-Biol. Chem 1 (1997) 65.
[6] C. Fleck, A. Janz, F. Schweitzer, E. Karge, M. Schwertfeger, G. Stein, Kidney Int. 59 (2001) 14.
[7] H. Matsuoka, S. Itoh, M. Kimoto, K. Kohno, O. Tamai, Y. Wada, H. Yasukawa, G. Iwami, S. Okuda, T. Imaizumi, Hypertension 29 (1997) 242.
[8] C. Fleck, F. Schweitzer, E. Karge, M. Busch, G. Stein, Clin. Chim. Acta 336 (2003) 1.
[9] S.M. Bode-Böger, R.H. Böger, S. Kienke, W. Junker, J.C. Fröhlich, Biochem. Biophys. Res. Commun. 219 (1996) 598.
[10] F. Abbasi, T. Asagmi, J.P. Cooke, C. Lamendola, T. McLaughlin, G.M. Reaven, M. Stuehlinger, P.S. Tsao, Am. J. Cardiol. 88 (2001) 1201.
[11] W.R. Feathers, Q.R. Rogers, R.A. Freedlan, Am. J. Physiol. 224 (1973) 127.
[12] P. Prados, H. Matsunaga, T. Mori, T. Santa, T. Fukushima, H. Homma, C. Kasai, K. Imai, Biomed. Chromatogr. 13 (1999) 27.
[13] E. Tyihak, S. Ferenczi, I. Hazai, S. Zoltan, A. Patthy, J. Chromatogr. 102 (1974) 257.
[14] M. Reporter, J.L. Corbin, Biochem. Biophys. Res. Commun. 43 (1971) 644.
[15] W.K. Paik, S. Kim, Biochem. Biophys. Res. Commun. 27 (1967) 479.
[16] Y. Kakimoto, Biochim. Biophys. Acta 243 (1971) 31.
[17] M. Kimoto, G.S. Whitley, H. Tsuji, T. Ogawa, J. Biochem. 117 (1995) 237.
[18] L.F. Huang, F.Q. Guo, Y.Z. Liang, Q.N. Hu, B.M. Cheng, Anal. Chim. Acta 487 (2003) 145.
[19] J. Martens-Lobenhoffer, S.M. Bode-Böger, J. Chromatogr. B 798 (2003) 231.
[20] E. Caussé, N. Siri, J.F. Arnal, C. Bayle, P. Malatray, P. Valdiguié, R. Salvayre, F. Couderc, J. Chromatogr. B 741 (2000) 77.
[21] A. Petterson, L. Uggla, V. Backman, J. Chromatogr. B 692 (1997) 257.
[22] B. Chen, L. Xia, R. Zhao, J. Chromatogr. B 692 (1997) 467.
[23] T. Teerlink, R.J. Nijveldt, S. de Jong, P.A.M. van Leeuwen, Anal. Biochem. 303 (2002) 131.
[24] Y. Dobashi, T. Santa, K. Nakagomi, K. Imai, Analyst 127 (2002) 54.
[25] J. Pi, Y. Kumagai, G. Sun, N. Shimojo, J. Chromatogr. B 742 (2000) 199.
[26] K. Imai, Y. Watanabe, Anal. Chim. Acta 130 (1981) 377.
[27] M. Marra, A.R. Bonfigli, R. Testa, I. Testa, A. Gambini, G. Coppa, Anal. Biochem. 318 (2003) 13.

Brief Definitive Report

Bone Marrow Allograft Rejection Mediated by a Novel Murine NK Receptor, NKG2I

Junzo Koike,[1] Hiroshi Wakao,[3] Yuko Ishizuka,[3] Taka-aki Sato,[4] Masaru Hamaoki,[4] Ken-ichiro Seino,[3,5] Haruhiko Koseki,[3] Toshinori Nakayama,[2] and Masaru Taniguchi[1,3]

[1]*Department of Molecular Immunology and* [2]*Department of Medical Immunology, Graduate School of Medicine, Chiba University, Chiba City, Chiba 260-8670, Japan*

[3]*Institute of Physical and Chemical Research, Research Center for Allergy and Immunology, Yokohama City, Kanagawa 230-0045, Japan*

[4]*Department of Diagnostics, YAMASA Corporation, Choshi, Chiba 288-0056, Japan*

[5]*PRESTO, Japan Science and Technology Corporation, Saitama 332-0012, Japan*

Abstract

Natural killer (NK) cells mediate bone marrow allograft rejection. However, the molecular mechanisms underlying such a rejection remain elusive. In previous analyses, it has been shown that NK cells recognize allogeneic target cells through Ly-49s and CD94/NKG2 heterodimers. Here, we describe identification and characterization of a novel murine NK receptor, NKG2I, belonging to the NKG2 family. NKG2I, which was composed of 226 amino acids, showed ~40% homology to the murine NKG2D and CD94 in the C-type lectin domain. Flow cytometric analysis with anti-NKG2I monoclonal antibody (mAb) revealed that expression of NKG2I was largely confined to NK and NKT cells, but was not seen in T cells. Furthermore, anti-NKG2I mAb inhibited NK cell–mediated cytotoxicity, whereas cross-linking of NKG2I enhanced interleukin 2– and interleukin 12–dependent interferon-γ production. Similarly, the injection of anti-NKG2I mAb before the allogeneic bone marrow transfer in vivo impinged on the function of NKG2I, resulting in the enhanced colony formation in the spleen. NKG2I is a novel activating receptor mediating recognition and rejection of allogeneic target cells.

Key words: C-type lectin family • NK cells • activating receptor • IFN-γ • NKT cells

Introduction

NK cells act as a first line of defense in innate immunity and also mediate rejection of allogeneic target cells, such as BM allografts (1, 2). NK cell function is exquisitely controlled by the orchestration of signals from stimulatory and inhibitory NK receptors, which recognize MHC class I–related molecules on target cells (3, 4). NK receptors have been categorized into three groups based on their structural and sequence homology. The first is the killer cell inhibitory receptors, belonging to the Ig superfamily, which are expressed in humans but not in rodents (5, 6). The second group is the C-type lectinlike Ly-49 receptors present solely in rodents (7). The third is the lectinlike homo- and heterodimer receptors, consisting of CD94 and a member of NKG2 family; they are observed both in humans and in rodents (8–10). Killer cell inhibitory receptors and Ly-49s recognize classical MHC class I molecules, whereas NKG2 family receptors bind nonclassical MHC class I molecules (11–13).

Regarding the role of NK receptors in NK cell–mediated allorejection, involvement of the NK receptors, such as CD94 and Ly-49, has been reported. Blocking the function of CD94 with anti-CD94 mAb enhances the in vitro cytotoxicity of C57BL/6 NK cells against BALB/c Con A lymphoblast target cells (14), implying that CD94, most likely together with NKG2A, may recognize the Qa-1 on the target cells. In addition, anti–Ly-49D mAb treatment results in eradication of a Ly-49D$^+$ subset in lethally irradiated C57BL/6 mice that, in turn, abrogates the ability to reject H-2D^d BM graft (15). In the present paper, we report identification and characterization of a novel murine

The online version of this article includes supplemental material.

Address correspondence to Masaru Taniguchi, Dept. of Molecular Immunology, Graduate School of Medicine, Chiba University, 1-8-1 Inohana, Chuoku, Chiba City, Chiba 260-8670, Japan. Phone: 81-43-226-2184; Fax: 81-43-227-1498; email: taniguti@med.m.chiba-u.ac.jp

NKG2 family receptor, NKG2I. We show that NKG2I acts as an activating receptor and mediates allorecognition and subsequent cytotoxic activity.

Materials and Methods

Animals. C57BL/6, BALB/c, C3H/HeN, ICR nu/nu mice, and Fisher rats were obtained from Charles River Laboratories. DBA/2Cr, AKR/N, (BALB/c × C57BL/6) F1, and 129/svJ mice were obtained from SLC and Jackson Laboratory, respectively. All experiments were performed in accordance with our institutional guidelines.

Identification of NKG2I through the Library Subtraction. PCR-Select cDNA subtraction kit (CLONTECH Laboratories, Inc.) was used to generate a library enriched for genes expressed in NKT cells over T cells. In brief, T cells were purified from the spleen of Jα281 knockout mice (16), and NKT cells were purified by FACSVantage™ cell sorter (Becton Dickinson) with α-galactosylceramide/CD1-d tetramer staining from the spleen of C57BL/6 mice. Purity of sorted cells was estimated to be >98%. In subtraction, T cell cDNA was used as a tester, whereas that of NKT cells was used as a driver. After subtraction, 1,000 clones were sequenced and analyzed by virtual Northern blot analysis.

Generation of Anti-NKG2I Monoclonal Antibodies. Fisher rats were injected with a fusion protein consisting of the extracellular portion of NKG2I and the Fc region of the human immunoglobulin. Spleen cells were fused to the SP2/O-Ag14 fusion partner. Hybridoma supernatants were screened for the staining ability of NKG2I-transfected COS7 cells by flow cytometric analysis. Five clones were established as follows: 3G7 (IgG1/κ), 5C6 (IgG1/κ), 7E8 (IgG2a/κ), 9D5 (IgG2a/κ), and 9F2 (IgG2a/κ). The mAbs were purified from ascites with protein G–Sepharose 4B and conjugated with biotin, FITC, and Cy5 with commercial kits.

Antibodies and cDNA. Anti-NKG2D antibody, murine CD94, NKG2C, E, D, DAP12, and DAP10 cDNA were provided by D.H. Raulet (University of California, Berkeley, Berkeley, CA). All other antibodies were obtained from BD Biosciences.

NK Cell Preparation and Stimulation by Anti-NKG2I mAb. Splenic NK cells were enriched with anti-DX5 Ab using the AutoMACS™ (Miltenyi Biotec). For stimulation experiments, NK cells were further purified as $NK1.1^+CD3^-$ cells to >90% by depleting $CD4^+$, $CD8^+$, $CD3^+$, $Gr\text{-}1^+$, $Ter\text{-}119^+$, and $CD19^+$ cells. NK cells (10^5 cells/well) were incubated for 24 h with or without IL-2 and IL-12 in 96-well plates precoated with 10 μg/ml of mAb, and the concentration of IFN-γ was measured by ELISA.

Cytotoxic Assay against Con A Lymphoblasts. Con A lymphoblasts were generated by stimulation of spleen cells with 2 μg/ml Con A (Sigma-Aldrich) for 48 h. Cytotoxic activities of IL-2–expanded NK cells (cultured for 1 wk) against Con A lymphoblasts were measured by a standard ^{51}Cr release assay. The specific lysis was calculated as follows: percent-specific lysis = ^{51}Cr cpm [(experimental release − spontaneous release)/(maximum release − spontaneous release)] × 100.

Biochemistry. IL-2–expanded NK cells were surface labeled with ^{125}I (Amersham Biosciences) using lactoperoxidase and lysed with buffer (1% NP-40, 50 mM Tris, 150 mM NaCl, 1 mM EDTA, and the protease inhibitor cocktail). The cell lysates were incubated with the 7E8-coated protein G–Sepharose 4 FF (Amersham Biosciences) and washed extensively. The samples were separated on an SDS-PAGE, and bands were visualized using the Bio Image Analyser (model BAS2500; Fuji Film).

Assay for BM Engraftment. Recipient C57BL/6 or (BALB/c × C57BL/6) F1 mice irradiated at 9.5 Gy were received intravenously with BALB/c or C57BL/6 BM cells. Spleen was removed and fixed with the Bouin's fixative on day 8, and the colony number was counted.

GenBank Accession No. The NKG2I sequence has been deposited in GenBank/EMBL/DDBJ under accession no. AF306663.

Online Supplemental Material. Table S1 summarizes the results of cDNA subtraction (NKT vs. T cells), and Figs. S1 and S2 show the control experiments using anti-asialo GM1 and anti-NKG2I. Online supplemental material is available at http://www.jem.org/cgi/content/full/jem.20030851/DC1.

Results and Discussion

A Novel NK Receptor Belonging to NKG2 Family. NKG2I was originally identified as a gene expressed preferentially in NKT cells over T cells by subtractive hybridization. Analysis of subtracted cDNA revealed that NK receptors, such as NKG2A/B, NKRP1-C, and NKG2D, were preferentially expressed in NKT cells (Table S1, available at http://www.jem.org/cgi/content/full/jem.20030851/DC1). A novel clone, preferentially expressed in NK and NKT cells, showed an extensive homology to the NK receptors and was subjected to further analysis (Figs. 1 and 2 A).

Putative proteins deduced from the nucleotide sequence consisted of 226 amino acids with four structural domains as follows: cytoplasmic (1-68), transmembrane (69-93), stalk (94-109), and C-type lectin domain (CTLD; 110-226) (Fig. 2 A). Sequence comparison indicated that NKG2I was a novel NK receptor belonging to the NKG2 family. In fact, the CTLD within NKG2I showed ~40% homology to that of murine NKG2D and CD94. Moreover, the residues in NKG2I, which may be engaged in disulfide bond formation (Fig. 2 A, closed circles) and in receptor dimerization (Fig. 2 A, closed circles and arrowheads), are readily inferred from the crystal structures of CD94 and NKG2D (17, 18). These data suggest that the CTLD in NKG2I possesses a higher order structure similar to CD94 and NKG2D. Nevertheless, NKG2I lacks any signaling motifs and positively charged amino acids in its putative transmembrane region, which are required for association with adaptor molecules such as FcεRIγ, CD3ζ, DAP10, and DAP12 (Fig. 2 A; references 19, 20).

Ligands for other members of the murine NKG2 receptors are MHC class I–related molecules as follows: Qa-1 for

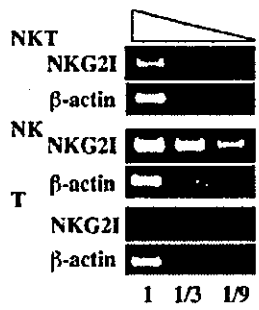

Figure 1. Preferential expression of NKG2I in NK and NKT cells over T cells. NKG2I expression was assessed by RT-PCR. β-actin serves as input cDNA control. Threefold serial dilution of cDNA was used.

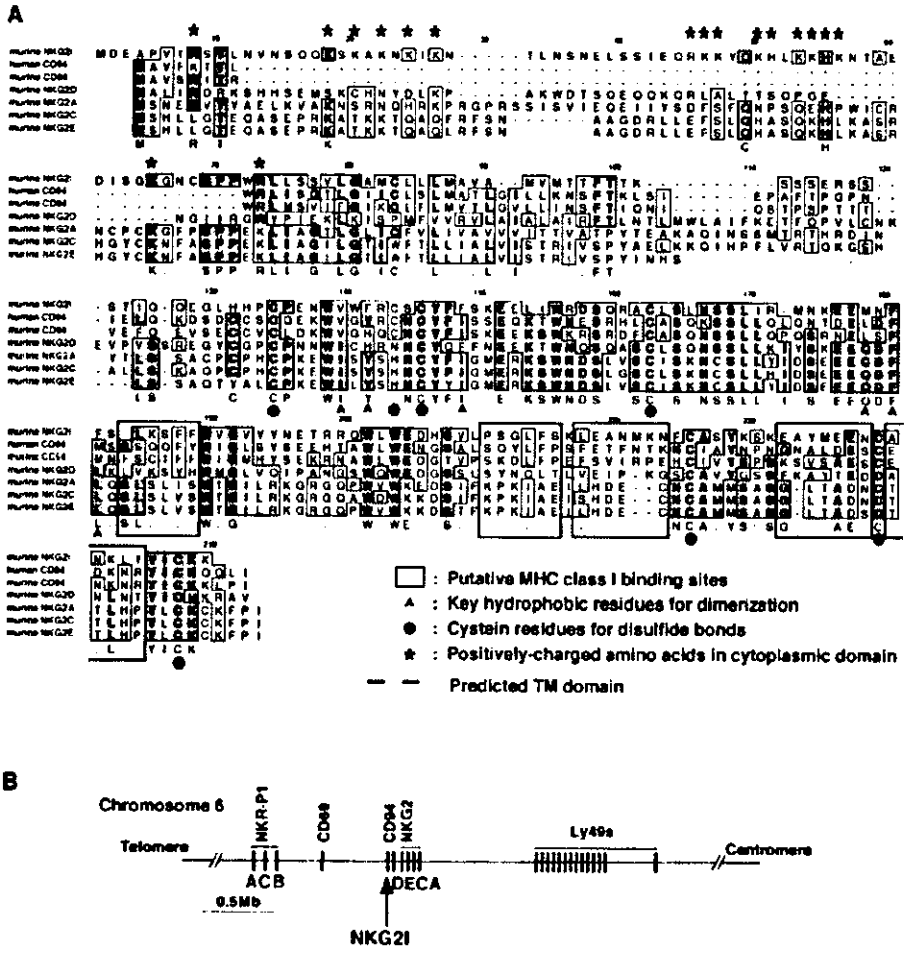

Figure 2. Characterization of NKG2I. (A) Alignment of the murine NKG2 family NK receptors and human CD94. The amino acid sequences of the murine NKG2 family receptors and human CD94 are aligned using the ClustalW algorithm. Highly conserved residues are displayed in the dark shaded boxes and depicted as consensus amino acids below the alignment. Similar amino acids are shown in light shaded boxes and are indicated with dots. The dotted line indicates the predicted transmembrane region using the TMpred program in EMBnet (http://www.ch.embnet.org). The squares indicate the putative ligand-binding site based on the crystal structure of the human CD94. The arrowheads show the hydrophobic residues responsible for dimerization. The closed circles indicate the cysteins involved in inter- and/or intramolecular disulfide bonding. The asterisks exhibit the positively charged amino acids in the cytoplasmic domain. (B) Genomic map of the murine NK gene complex. The map is presented schematically based on the mouse genome sequence from the National Center for Biotechnology Information. The relative location of the NKG2I is indicated by the arrow.

CD94/NKG2 heterodimers (21, 22) and Raes, H60, and MULT1 for NKG2D homodimers (23–25). As NKG2I exhibits little similarity in a putative ligand binding domain to other NK receptors (Fig. 2 A, squares), it may recognize ligands distinct from those aforementioned (17, 18). An abundance of positively charged amino acids in the cytoplasmic domain of NKG2I points to the possibility that it may associate with novel adaptors responsible for signal transduction (Fig. 2 A, asterisks).

DNA sequence analysis of NKG2I in the National Center for Biotechnology Information mouse genome database revealed that NKG2I maps adjacent to the CD94/NKG2 gene cluster and between CD69 and CD94 in NK receptor gene complex on murine chromosome 6 (Fig. 2 B). Curiously, no human orthologue of NKG2I was found, suggesting that this receptor may be unique to rodents.

Characterization of NKG2I by the mAbs. To characterize NKG2I, we established several mAbs specific for NKG2I (Fig. 3 A). These mAbs stained NKG2I-transfected COS7 cells specifically, and did not cross react with CD94, NKG2A/C/E, or NKG2D molecules (Fig. 3 A). Staining with 3G7 mAb revealed that most NK ($NK1.1^+CD3^-$) cells in the spleen (84%), BM (74%), and liver (77%) expressed NKG2I (Fig. 3 B). NKG2I was also expressed on a subset of NKT ($NK1.1^+CD3^+$) cells, the expression levels of which varied significantly among tissues (ranging from 13 to 54%), but was barely detected on T ($NK1.1^-CD3^+$) cells (Fig. 3 B).

Because the expression of NKG2 varies depending on mouse strains (14), we examined whether this is also the case for NKG2I. Flow cytometric analysis showed that NKG2I as well as CD94 and NKG2A/C/E expressions were found regardless of strains (Fig. 3 C, C57BL/6, BALB/c, C3H/HeN, DBA/2Cr, AKR/N, and 129/svJ). However, the expression level of NKG2I differed among the strains, implying the "calibration" of this receptor (26). Moreover, the cDNA sequence for NKG2I from these strains revealed that they encoded an identical amino acid, suggesting that NKG2I is an invariant molecule on NK cells and exhibits an expression profile distinct from that of Ly-49s, which carry allelic polymorphisms (27).

Biochemical analysis with ^{125}I-labeled NK cells followed by immunoprecipitation with anti-NKG2I mAb (7E8) revealed that NKG2I migrated predominantly as a ~96-kD protein under nonreducing conditions, whereas a prominent

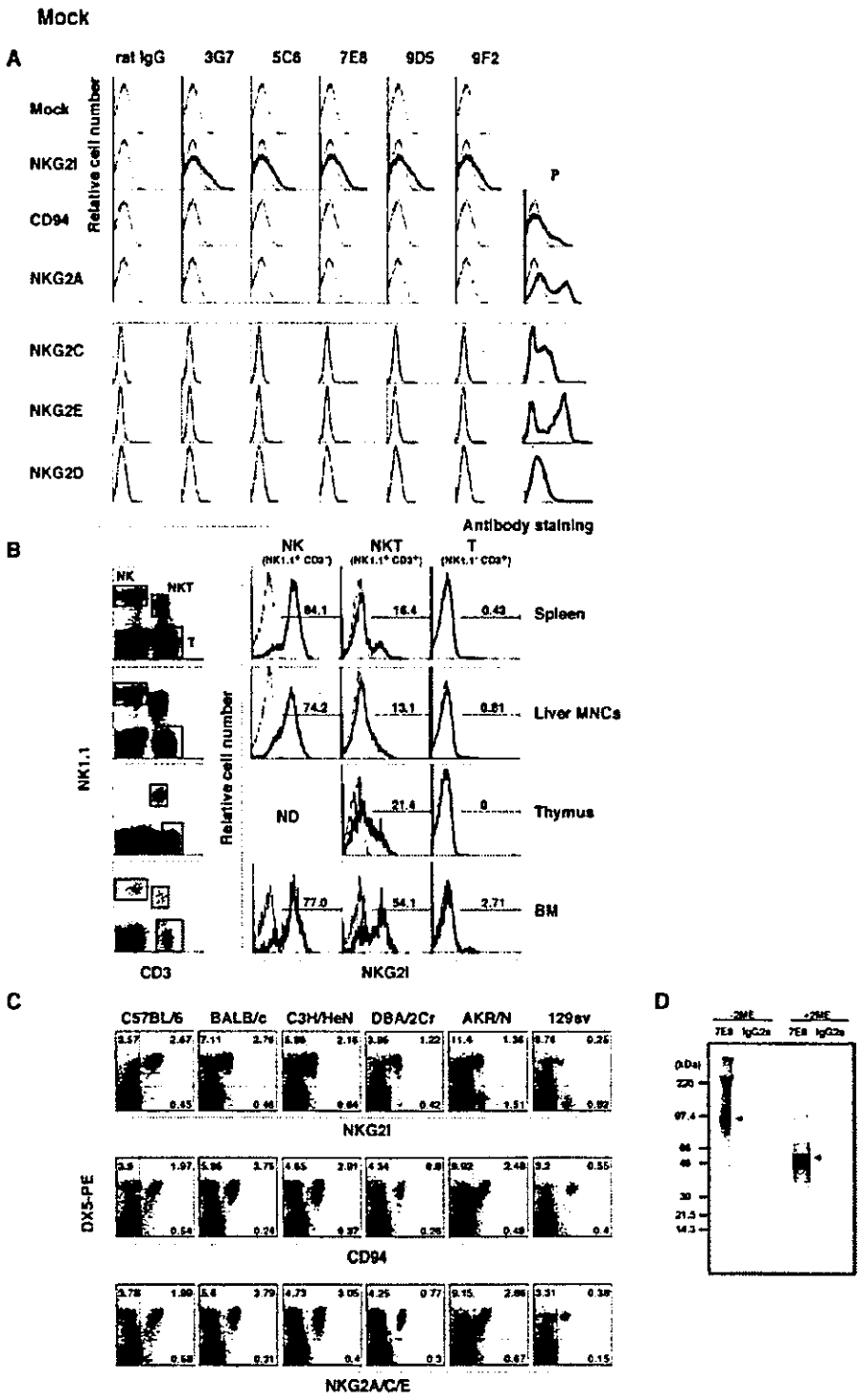

Figure 3. Characterization of anti-NKG2I monoclonal antibodies. (A) Establishment of the mAbs against NKG2I. COS7 cells were transiently transfected with mock, NKG2I, murine CD94, NKG2A/C with CD94, NKG2E with DAP12, and NKG2D with DAP10 cDNA expression vector. Cells were harvested 48 h later and incubated with the biotin-conjugated 3G7, 5C6, 7E8, 9D5, 9F2, or control rat IgG, followed by staining with the FITC-streptavidin (thick histogram). For CD94, NKG2A/C/E, and NKG2D transfectants, cells were incubated with the biotin-conjugated anti-CD94 mAb or with the anti-NKG2A/C/E or anti-NKG2D mAb as positive control (P, thick histogram). Background staining is shown as thin histograms. (B) Expression of NKG2I in the various lymphoid subsets. Spleen, liver mononuclear cells, thymocytes, and BM cells from C57BL/6 mice were stained with the FITC–anti-NKG2I (3G7), PE-NK1.1, and Cy5–anti-CD3. The expression of NKG2I in the gated lymphoid subsets for NK ($NK1.1^+CD3^-$), NKT ($NK1.1^+CD3^+$), or T ($NK1.1^-CD3^+$) cells is shown as histogram (thick lines) overlaid with the background staining (thin lines). The percentage of $NKG2I^+$ cells in each lymphoid subset is shown. (C) Expression of the NKG2I, CD94, and NKG2A/C/E in the various strains of mice. Spleen cells from the different mouse strains were stained with PE-DX5 together with biotin–anti-NKG2I (3G7), anti-CD94, or anti-NKG2A/C/E mAb followed by FITC-streptavidin. Percentage of cells in each subset is shown. (D) NKG2I exists as a dimer with the disulfide bond. C57BL/6 NK cells expanded with IL-2 were surface labeled with ^{125}I and immunoprecipitated with the anti-NKG2I mAb (7E8) or rat IgG2a. Immunoprecipitated proteins were separated on an SDS-PAGE under nonreducing (in the absence of 2-mercaptoethanol [−2ME]) or reducing (in the presence of 2-mercaptoethanol [+2ME]) conditions, and visualized with BAS2500.

~48-kD band emerged under reducing conditions on an SDS-PAGE (Fig. 3 D, arrowheads). This suggests that NKG2I forms homo- or heterodimer-like other NKG2 family members (21, 23, 24). Because its predicted molecular weight is 26,265, it is conceivable that NKG2I is covalently modified, though its precise nature has yet to be examined.

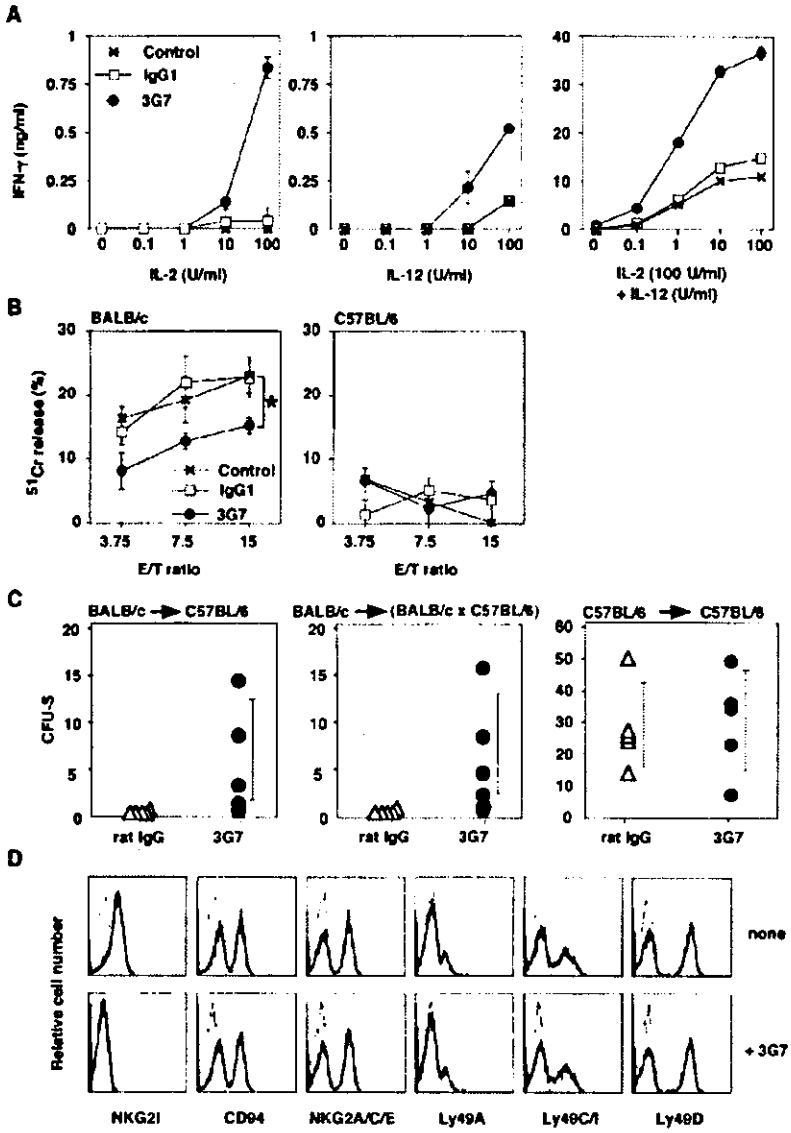

Figure 4. NKG2I functions as an activating NK receptor in allograft rejection. (A) IFN-γ production upon cross-linking of NKG2I in NK cells. NK cells from C57BL/6 spleen were incubated in the presence of IL-2, IL-12, or IL-2/IL-12 in the plate immobilized with 3G7 or rat IgG1. Control experiments were done without any antibody. The concentrations of IFN-γ in the culture supernatant are shown. Data are indicated as mean ± SD from three independent experiments. (B) 3G7 mAb inhibits the cytotoxicity of NK cells against the allogeneic target cells. The cytolytic activity of C57BL/6 NK cells expanded with IL-2 was determined in the presence of 10 μg/ml of 3G7 mAb or control rat IgG1. Control experiments were done without any antibody. Con A lymphoblasts prepared from BALB/c (left) or C57BL/6 (right) mice were used as target cells. Data are shown as mean ± SD from three independent experiments (n = 6/experiment). *, $P < 0.05$ as compared 3G7 mAb versus rat IgG1 at the indicated E/T ratio. (C) Blocking the NKG2I function compromises rejection of the allogeneic BM cell transplantation. Responder C57BL/6 or (BALB/c × C57BL/6) F1 mice were treated with 100 μg of 3G7 mAb or rat IgG before BM transplantation with 3×10^6 cells (for C57BL/6 recipients) or 0.1×10^6 cells (for F1 recipients) from BALB/c or C57BL/6, and received the same amount of each of the Abs on days 3 and 6. The number of colonies in the spleen of the recipient mice (n = 5) was counted 8 d after BM transfer. The error bars represent the standard deviation, and representative data from three independent experiments are shown. (D) Blocking the function of NKG2I does not interfere with the expression of other NK receptors. The effect of 3G7 mAb on the expression of other NK receptors relevant to the allorejection was evaluated by flow cytometric analysis on NK cells. C57BL/6 mice were left untreated (top) or treated with 100 μg/body of 3G7 (bottom) for 1 h. NK ($NK1.1^+CD3^-$) cells were stained with the biotin-anti-NKG2I (7E8), biotin-anti-CD94, biotin-anti-NKG2A/C/E, biotin-anti-Ly49A, biotin-anti-Ly49C/I, or FITC-anti-Ly49D, respectively. Biotin-conjugated Ab was visualized with FITC-streptavidin. Expression of each NK receptor is shown as histogram (thick lines) overlaid with background staining (thin lines).

NKG2I Acts as an Activating Receptor in Allorejection. Given that NKG2I is expressed predominantly in NK cells (Fig. 3 B) and that CD94, which is quite similar to NKG2I, is implicated in recognition of allogeneic target cells (14), we hypothesized that NKG2I also plays a role in NK cell–mediated allorecognition and subsequent cytotoxic activity. Because activating signals elicited from NK receptors often lead to cytokine production and/or activation of cytotoxicity (28), the function of NKG2I was assessed by measuring IFN-γ production (Fig. 4 A). Cross-linking of NKG2I with 3G7 mAb led to induction of IFN-γ in the presence of either IL-2 or IL-12 in a cytokine dose-dependent manner and their synergistic effects were observed (Fig. 4 A, right). These results indicate that NKG2I cross-linking enhances the extent of IL-2– and IL-12–elicited signaling leading to IFN-γ production. Thus, NKG2I may serve as an activating NK receptor.

We explored the function of NKG2I through an in vitro cytolytic assay with 3G7 mAb (Fig. 4 B). C57BL/6 NK cells lysed allogeneic BALB/c but not syngeneic C57BL/6 Con A lymphoblast target cells (Fig. 4 B). In contrast, treatment of C57BL/6 NK cells with 3G7 mAb inhibited cytolytic activity against BALB/c target cells significantly, whereas control Ab showed little effect (Fig. 4 B, left).

Allogeneic BM cell transplantation experiments further confirmed these results (Fig. 4 C). BALB/c BM cells administrated into lethally irradiated C57BL/6 mice (BALB/c into C57BL/6) were rejected in a manner dependent on

NK cells, and no colony derived from the transplanted cells appeared in the spleen of recipient mice as reported (Fig. 4 C, left; reference 29). In contrast, administration of 3G7 mAb but not the control anti–rat IgG Ab into the recipient C57BL/6 mice before BALB/c BM transfer suppressed the rejection of BALB/c BM grafts and resulted in a significant number of colony formations in the spleen (Fig. 4 C, left). Similarly, (BALB/c × C57BL/6) F1 mice as a recipient, whose T cells are tolerant to the parent BALB/c, showed significantly impaired rejection of BALB/c BM cells (BALB/c into F1) in the presence of 3G7 mAb (Fig. 4 C, middle). In contrast, no effects were observed in the syngeneic BM transplantation (Fig. 4 C, right, C57BL/6 into C57BL/6). These results indicate that NKG2I on NK cells recognizes putative ligands present on allogeneic BM cells and induces signals leading to the rejection of allografts.

It should be mentioned that administration of anti-NK1.1, anti–asialo GM1, or anti–Ly-49D mAb also abrogated the rejection of allogeneic BM grafts (Fig. S1, available at http://www.jem.org/cgi/content/full/jem.20030851/DC1), but these effects were primarily due to the depletion of NK cells expressing these molecules (15, 29). On the other hand, 3G7 mAb treatment did not change the number of NK cells in vivo (Fig. S2, available at http://www.jem.org/cgi/content/full/jem.20030851/DC1). More importantly, 3G7 mAb treatment did not alter the expression of other NK receptors, such as CD94, NKG2A/C/E, Ly-49A, Ly-49C/I, and Ly-49D, under the conditions that NKG2I expression was rapidly down-regulated in vivo (Fig. 4 D). These results suggest that allogeneic recognition and subsequent activation of NK cells leading to cytotoxic activity against allogeneic BM cells is attributed to NKG2I but not to modulation of other NK receptor expression.

In summary, we have identified and characterized a novel activating NK receptor that plays a crucial role in allograft rejection. Identification of the cognate ligands and elucidation of the signaling pathway of NKG2I will shed light on mechanisms underlying allogeneic recognition and rejection.

The authors thank Dr. D.H. Raulet for CD94, NKG2C, E, D, DAP12, and DAP10 cDNA and anti-NKG2D mAb; Ms. H. Tanabe for preparation; and Mr. R. Triendl and Ms. N.M. Maeshima for critical reading.

This work was supported by grants from the Ministry of Education, Culture, Sports, Science and Technology of Japan as follows: C13218016 (to T. Nakayama), A13307011 (to M. Taniguchi), B14370107 (to T. Nakayama), and C12670293 (to T. Nakayama). This work was also supported by the Special Coordination Funds for Promoting Science and Technology (to T. Nakayama); the Program for Promotion of Fundamental Studies in Health Sciences of the Organization for Pharmaceutical Safety and Research of the Ministry of Health, Labor and Welfare (to M. Taniguchi); and by the Human Frontier Science Program Research grant RG00168/2000-M206 (to M. Taniguchi). J. Koike is recipient of a Research Fellowships of the Japan Society for the Promotion of Science for Young Scientists (0000147313).

Submitted: 23 May 2003
Accepted: 5 November 2003

References

1. Murphy, W.J., V. Kumar, and M. Bennett. 1987. Rejection of bone marrow allografts by mice with severe combined immune deficiency (SCID). Evidence that natural killer cells can mediate the specificity of marrow graft rejection. *J. Exp. Med.* 165:1212–1217.
2. Trinchieri, G. 1989. Biology of natural killer cells. *Adv. Immunol.* 47:187–376.
3. Lanier, L.L. 1998. NK cell receptors. *Annu. Rev. Immunol.* 16:359–393.
4. Yokoyama, W.M. 1998. Natural killer cell receptors. *Curr. Opin. Immunol.* 10:298–305.
5. Colonna, M. 1997. Specificity and function of immunoglobulin superfamily NK cell inhibitory and stimulatory receptors. *Immunol. Rev.* 155:127–133.
6. Moretta, A., R. Biassoni, C. Bottino, D. Pende, M. Vitale, A. Poggi, M.C. Mingari, and L. Moretta. 1997. Major histocompatibility complex class I-specific receptors on human natural killer and T lymphocytes. *Immunol. Rev.* 155:105–117.
7. Raulet, D.H., W. Held, I. Correa, J.R. Dorfman, M.F. Wu, and L. Corral. 1997. Specificity, tolerance and developmental regulation of natural killer cells defined by expression of class I-specific Ly49 receptors. *Immunol. Rev.* 155:41–52.
8. Houchins, J.P., T. Yabe, C. McSherry, and F.H. Bach. 1991. DNA sequence analysis of NKG2, a family of related cDNA clones encoding type II integral membrane proteins on human natural killer cells. *J. Exp. Med.* 173:1017–1020.
9. Vance, R.E., D.M. Tanamachi, T. Hanke, and D.H. Raulet. 1997. Cloning of a mouse homolog of CD94 extends the family of C-type lectins on murine natural killer cells. *Eur. J. Immunol.* 27:3236–3241.
10. Glienke, J., Y. Sobanov, C. Brostjan, C. Steffens, C. Nguyen, H. Lehrach, E. Hofer, and F. Francis. 1998. The genomic organization of NKG2C, E, F, and D receptor genes in the human natural killer gene complex. *Immunogenetics.* 48:163–173.
11. Anderson, S.K., J.R. Ortaldo, and D.W. McVicar. 2001. The ever-expanding Ly49 gene family: repertoire and signaling. *Immunol. Rev.* 181:79–89.
12. Cerwenka, A., and L.L. Lanier. 2001. Ligands for natural killer cell receptors: redundancy or specificity. *Immunol. Rev.* 181:158–169.
13. Vilches, C., and P. Parham. 2002. KIR: diverse, rapidly evolving receptors of innate and adaptive immunity. *Annu. Rev. Immunol.* 20:217–251.
14. Toyama-Sorimachi, N., Y. Taguchi, H. Yagita, F. Kitamura, A. Kawasaki, S. Koyasu, and H. Karasuyama. 2001. Mouse CD94 participates in Qa-1-mediated self recognition by NK cells and delivers inhibitory signals independent of Ly-49. *J. Immunol.* 166:3771–3779.
15. Raziuddin, A., D.L. Longo, L. Mason, J.R. Ortaldo, M. Bennett, and W.J. Murphy. 1998. Differential effects of the rejection of bone marrow allografts by the depletion of activating versus inhibiting Ly-49 natural killer cell subsets. *J. Immunol.* 160:87–94.
16. Cui, J., T. Shin, T. Kawano, H. Sato, E. Kondo, I. Toura, Y. Kaneko, H. Koseki, M. Kanno, and M. Taniguchi. 1997. Requirement for Valpha14 NKT cells in IL-12-mediated rejection of tumors. *Science.* 278:1623–1626.
17. Boyington, J.C., A.N. Riaz, A. Patamawenu, J.E. Coligan, A.G. Brooks, and P.D. Sun. 1999. Structure of CD94 reveals a novel C-type lectin fold: implications for the NK cell–asso-

ciated CD94/NKG2 receptors. *Immunity*. 10:75–82.
18. Wolan, D.W., L. Teyton, M.G. Rudolph, B. Villmow, S. Bauer, D.H. Busch, and I.A. Wilson. 2001. Crystal structure of the murine NK cell-activating receptor NKG2D at 1.95 A. *Nat. Immunol.* 2:248–254.
19. Moretta, A., C. Bottino, M. Vitale, D. Pende, C. Cantoni, M.C. Mingari, R. Biassoni, and L. Moretta. 2001. Activating receptors and coreceptors involved in human natural killer cell-mediated cytolysis. *Annu. Rev. Immunol.* 19:197–223.
20. Lanier, L.L. 2001. On guard–activating NK cell receptors. *Nat. Immunol.* 2:23–27.
21. Vance, R.E., J.R. Kraft, J.D. Altman, P.E. Jensen, and D.H. Raulet. 1998. Mouse CD94/NKG2A is a natural killer cell receptor for the nonclassical major histocompatibility complex (MHC) class I molecule Qa-1(b). *J. Exp. Med.* 188: 1841–1848.
22. Vance, R.E., A.M. Jamieson, and D.H. Raulet. 1999. Recognition of the class Ib molecule Qa-1(b) by putative activating receptors CD94/NKG2C and CD94/NKG2E on mouse natural killer cells. *J. Exp. Med.* 190:1801–1812.
23. Diefenbach, A., A.M. Jamieson, S.D. Liu, N. Shastri, and D.H. Raulet. 2000. Ligands for the murine NKG2D receptor: expression by tumor cells and activation of NK cells and macrophages. *Nat. Immunol.* 1:119–126.
24. Cerwenka, A., A.B. Bakker, T. McClanahan, J. Wagner, J. Wu, J.H. Phillips, and L.L. Lanier. 2000. Retinoic acid early inducible genes define a ligand family for the activating NKG2D receptor in mice. *Immunity*. 12:721–727.
25. Carayannopoulos, L.N., O.V. Naidenko, D.H. Fremont, and W.M. Yokoyama. 2002. Cutting edge: murine UL16-binding protein-like transcript 1: a newly described transcript encoding a high-affinity ligand for murine NKG2D. *J. Immunol.* 169:4079–4083.
26. Olsson-Alheim, M.Y., M. Salcedo, H.G. Ljunggren, K. Karre, and C.L. Sentman. 1997. NK cell receptor calibration: effects of MHC class I induction on killing by Ly49Ahigh and Ly49Alow NK cells. *J. Immunol.* 159:3189–3194.
27. Ortaldo, J.R., A.T. Mason, R. Winkler-Pickett, A. Raziuddin, W.J. Murphy, and L.H. Mason. 1999. Ly-49 receptor expression and functional analysis in multiple mouse strains. *J. Leukoc. Biol.* 66:512–520.
28. Bakker, A.B., J. Wu, J.H. Phillips, and L.L. Lanier. 2000. NK cell activation: distinct stimulatory pathways counterbalancing inhibitory signals. *Hum. Immunol.* 61:18–27.
29. Tiberghien, P., D.L. Longo, J.W. Wine, W.G. Alvord, and C.W. Reynolds. 1990. Anti-asialo GM1 antiserum treatment of lethally irradiated recipients before bone marrow transplantation: evidence that recipient natural killer depletion enhances survival, engraftment, and hematopoietic recovery. *Blood*. 76:1419–1430.

THE JOURNAL OF BIOLOGICAL CHEMISTRY
Vol. 279, No. 3, Issue of January 16, pp. 1676–1683, 2004
Printed in U.S.A.

Ultraviolet A-induced Production of Matrix Metalloproteinase-1 Is Mediated by Macrophage Migration Inhibitory Factor (MIF) in Human Dermal Fibroblasts*

Received for publication, April 8, 2003, and in revised form, October 10, 2003
Published, JBC Papers in Press, October 27, 2003, DOI 10.1074/jbc.M303650200

Hirokazu Watanabe‡, Tadamichi Shimizu‡, Jun Nishihira§, Riichiro Abe‡, Toshinori Nakayama¶‖, Masaru Taniguchi‖, Hisataka Sabe‡‡, Teruo Ishibashi§, and Hiroshi Shimizu‡§§**

*From the Departments of ‡Dermatology and §Molecular Biochemistry, Hokkaido University Graduate School of Medicine, Kita-ku, Sapporo 060-8638, Japan, the ¶Department of Medical Immunology and ‖Department of Molecular Immunology, Graduate School of Medicine, Chiba University, 1-8-1 Inohana Chuo-ku, Chiba 260-8670, Japan, the **Laboratory for Immune Regulation, RIKEN Research Center for Allergy and Immunology, Yokohama, 230-0045, Japan, and the ‡‡Department of Molecular Biology, Osaka Bioscience Institute, Osaka 565-0874, Japan*

Matrix metalloproteinases (MMPs) are thought to be responsible for dermal photoaging in human skin. In the present study, we evaluated the involvement of macrophage migration inhibitory factor (MIF) in MMP-1 expression under ultraviolet A (UVA) irradiation in cultured human dermal fibroblasts. UVA (20 J/cm^2) up-regulates MIF production, and UVA-induced MMP-1 mRNA production is inhibited by an anti-MIF antibody. MIF (100 ng/ml) was shown to induce MMP-1 in cultured human dermal fibroblasts. We found that MIF (100 ng/ml) enhanced MMP-1 activity in cultured fibroblasts assessed by zymography. Moreover, we observed that fibroblasts obtained from MIF-deficient mice were much less sensitive to UVA regarding MMP-13 expression than those from wild-type BALB/c mice. Furthermore, after UVA irradiation (10 J/cm^2), dermal fibroblasts of MIF-deficient mice produced significantly decreased levels of MMP-13 compared with fibroblasts of wild-type mice. Next we investigated the signal transduction pathway of MIF. The up-regulation of MMP-1 mRNA by MIF stimulation was found to be inhibited by a PKC inhibitor (GF109203X), a Src-family tyrosine kinase inhibitor (herbimycin A), a tyrosine kinase inhibitor (genistein), a PKA inhibitor (H89), a MEK inhibitor (PD98089), and a JNK inhibitor (SP600125). In contrast, the p38 inhibitor (SB203580) was found to have little effect on expression of MMP-1 mRNA. We found that PKC-pan, PKCα/βII, PKCδ (Thr505), PKCδ (Ser^{643}), Raf, and MAPK were phosphorylated by MIF. Moreover, we demonstrated that phosphorylation of PKCα/βII and MAPK in response to MIF was suppressed by genistein, and herbimycin A as well as by transfection of the plasmid of C-terminal Src kinase. The DNA binding activity of AP-1 was significantly up-regulated 2 h after MIF stimulation. Taken together, these results suggest that MIF is involved in the up-regulation of UVA-induced MMP-1 in dermal fibroblasts through PKC-, PKA-, Src family tyrosine kinase-, MAPK-, c-Jun-, and AP-1-dependent pathways.

The skin is an important barrier that protects the body from damage due to direct contact with the outside environment, including trauma, bacterial infection, and ultraviolet (UV) irradiation. Regarding the environmental damage to skin, the most common physical injury is that caused by UV irradiation. UV irradiation substantially increases the risk of actinic damage to the skin. Interstitial collagens, the major structural components of the dermis, have been found to be particularly diminished in skin actinically damaged by UV irradiation (1–3). Quantitative and qualitative changes in the dermal extracellular matrix proteins such as elastin, glycosaminoglycans, and interstitial collagens are also associated in dermal photodamage. There are several morphological and biochemical indications that collagen type I is reduced in UV actinically damaged skin (4). Various types of UV-induced matrix-degenerating metalloproteinases present in dermal fibroblasts contribute to the breakdown of dermal interstitial collagen and other connective tissue components.

As for the underlying biological mechanisms of action involved in skin damage, the skin is known to secrete a number of cytokines, including interleukin (IL)[1]-1, IL-6, and tumor necrosis factor (TNF)-α (5–7). UV irradiation up-regulates the production of these cytokines, and UV-induced collagenases such as matrix metalloproteinase (MMP)-1 from dermal fibroblasts are mediated in part by IL-1α and IL-1β (6). Furthermore, collagenase activity has been shown to be inhibited by a tissue inhibitor of metalloproteinases (TIMP) (8).

Macrophage migration inhibitory factor (MIF), originally identified as a lymphokine that concentrates macrophages at inflammatory loci, is a potent activator of macrophages *in vivo* and is considered to play an important role in cell-mediated immunity (9, 10). It has been reported that MIF is expressed primarily by T cells and macrophages; recent studies have however revealed that this protein is ubiquitously expressed by various cells, thus indicating its involvement beyond the immune system in a variety of pathologic states (11, 12). It is of interest that MIF functions as a cytokine, an anterior pitu-

* This work was supported in part by Grants-in-aid for research (No. 11670813 and 13357008) from the Ministry of Education, Science, and Culture of Japan, and the Shiseido Foundation for Skin Aging Research. The costs of publication of this article were defrayed in part by the payment of page charges. This article must therefore be hereby marked "*advertisement*" in accordance with 18 U.S.C. Section 1734 solely to indicate this fact.

§§ To whom correspondence should be addressed: Dept. of Dermatology, Hokkaido University Graduate School of Medicine, Sapporo 060-8638, Japan. Fax: 81-11-706-7820; E-mail: shimizu@med.hokudai.ac.jp.

[1] The abbreviations used are: IL, interleukin; MIF, macrophage migration inhibitory factor; MMP, matrix metalloproteinase; UV, ultraviolet; TNF-α, tumor necrosis factor-α; TIMP, tissue inhibitor of matrix metalloproteinase; JNK, c-Jun N-terminal kinase; EMSA, electrophoretic gel mobility shift assay; CSK, C-terminal Src kinase; PKC, protein kinase C; FCS, fetal calf serum; DMEM, Dulbecco's modified Eagle's medium; WT, wild type; ELISA, enzyme-linked immunosorbent assay; MAPK, mitogen-activated protein kinase; DAG, diacylglycerol-PKA, cAMP-dependent protein kinase.

itary-derived hormone, and a glucocorticoid-induced immunomodulator (13).

It is of note that UVA irradiation reaches the reticular dermis, rendering fibroblasts accessible targets (14). In the skin, MIF is expressed in the epidermis, particularly in the basal layer (15). However, the precise role of MIF in the dermis and the effects of UVA on MIF expression of dermal fibroblasts remain unknown. In the present study, we attempted to determine whether MIF mediates the up-regulation of MMP-1 expression in response to the stimulation of UVA irradiation. We also investigated the signal transduction pathway of MIF in human dermal fibroblasts.

EXPERIMENTAL PROCEDURES

Materials—The following materials were obtained from commercial sources. Genistein, herbimycin A, PP2, GF109203X, H89, PD98089, SB203580, and SP600125 were purchased from Calbiochem (San Diego, CA); Dulbecco's modified Eagle's medium (DMEM) from Invitrogen (Groningen, Netherland); Dig Gel Shift kit and FuGENE 6 was from Roche Applied Science (Mannheim, Germany); the Isogen RNA extraction kit was from Nippon Gene (Toyama, Japan); the Biotrack MMP-1 assay kit, [α-^{32}P]dCTP, and Hybond N nylon membrane were from Amersham Biosciences (Piscataway, NJ); the consensus AP-1 oligonucleotide was from Promega (Madison, WI); the DNA random primer labeling kit was from Takara (Kyoto, Japan); anti-phospho-PKCpan, PKCα/βII (Thr$^{638/641}$), PKCδ (Thr^{505}), PKCδ (Ser^{643}), PKCθ (Thr^{538}), PKD/PKCμ (Ser$^{744/748}$), PKD/PKCμ (Ser^{916}), PKCζ/λ (Thr$^{410/403}$); anti-phospho-Raf, anti-phospho-p44/p42 MAPK antibodies, and the phototope-HRP Western blot detection system were from Cell Signaling Technology (Beverly, MA); Anti-MMP-1, anti-β-actin antibodies and gelatin were purchased from Sigma-Aldrich Co.; anti-MMP-13 (Collagenase-3) antibody was from Chemicon (Temecula, CA); YM-30 was from Millipore (Bedford, MA); and recombinant human MMP-1 was from Genzyme-Techne (Minneapolis, MN). The anti-MIF polyclonal antibody was prepared as described previously (15). Recombinant human MIF was expressed in *Escherichia coli* BL21/DE3 (Novagen, Madison, WI) and purified as described previously (16). This MIF contained less than 1 pg of endotoxin per μg of protein, as determined by chromogenic Lumulus amoebocyte assay (BioWhittaker, Walkerville, MD). Plasmids of C-terminal Src kinase (CSK) and dominant negative mutant of CSK (CSK$^-$) were prepared as previously described (17).

Cells and Skin Tissues—Human dermal fibroblasts were purchased from Dainippon Seiyaku (Osaka, Japan). Cells of passages 3–4 were used for the experiments. In brief, cells were maintained in DMEM supplemented with 10% heat-inactivated FCS, glutamine (2 mM), sodium ascorbate (50 μg/ml), penicillin (100 units/ml), streptomycin (100 μg/ml), and fungizone (100 μg/ml). The cells were grown in a moist atmosphere in a 5% CO_2 incubator at 37 °C.

MIF-deficient mice were established by targeted disruption of the MIF gene, using a mouse strain bred onto a BALB/c background (18). Wild-type (WT) BALB/c mice were purchased from Japan Clea (Shizuoka, Japan) and maintained under specific-pathogen-free conditions. Mouse dermal fibroblasts were obtained from MIF-deficient mice and control WT mice. Newborn mouse skin was carefully shaven, a segment of skin excised, and fibroblasts were obtained using the standard explant technique. Briefly, the skin was cut into 3 × 5-mm pieces and placed onto large Petri dishes with the subcutaneous side down. Once a sufficient number of fibroblasts had migrated out from the skin sections, pieces of the skin were removed and the cells were passaged by trypsin digestion in the same manner as for the fibroblasts. Fibroblasts were grown in DMEM containing 10% FCS and penicillin/streptomycin. The cells from passage 3 were used for the experiment.

UVA Irradiation—Human dermal fibroblasts were washed twice with phosphate-buffered saline. The UVA irradiation source was a FL20S/BLB fluorescent lamp (Clinical Supply, Tokyo, Japan) that emitted an energy spectrum with high fluency in the UVA region (300–430 nm), with a peak at 352 nm. A 6-mm thick glass plate was used to block UVB emissions. The emitted dose was calculated using a UVA radiometer photodetector (Torex, Tokyo, Japan). The cells were washed with phosphate-buffered saline, suspended in Hank's buffer, and subjected to UVA irradiation. The duration of UV irradiation delivered to cells was altered by sliding a plastic lid covered with aluminum foil onto a flat-bottomed 6-well plate. After irradiation, the cells were cultured in DMEM with 10% FCS at 37 °C. Control samples were mock-irradiated and maintained under the same culture conditions as those used for the UVA-irradiated specimens. To examine the effects of anti-MIF antibody on the UVA-induced MMP-1 mRNA, fibroblasts were UVA-irradiated (20 J/cm^2) in the presence of an anti-MIF antibody (1 and 10 μg/ml) in DMEM supplemented with 10% FCS and then further incubated for 24 h. Expression of MMP-1 mRNA and protein levels were assessed by Northern blot and Western blot analyses. The abdomens of MIF-deficient mice or WT mice were carefully shaved, and irradiated with UVA (0–30 J/cm^2). After UVA irradiation for 24 h, skin was surgically obtained and MMP-13 production was assessed by Western blot analysis. Dermal fibroblasts from MIF-deficient mice or WT mice were harvested after reaching 70% confluence. The cells were washed twice with PBS and exposed to a UVA fluorescent lamp for the indicated doses (0–10 J/cm^2). After irradiation, cells were cultured in DMEM supplemented with 10% FCS for 24 h, and MMP-13 production was evaluated by Western blot analysis.

Northern Blot Analysis—Complete coding cDNA for human MMP-1 in a pSP64 vector was obtained from the American Type Culture Collection. Templates of human TIMP-1 and glyceraldehyde-3-phosphate dehydrogenase (GAPDH) cDNA for Northern blot analyses were obtained by reverse transcription-polymerase chain reaction (RT-PCR) from a human cDNA library of human primary dermal fibroblasts. Preparation of each template proceeded using the following primers: TIMP-1 (535 bp), forward primer 5′-TCCTGTTGTTGCTGTGGCTGATAGC-3′ and reverse primer 5′-CAGGCAAGGTGACGGGACTGGAAGC-3′, GAPDH (306 bp), forward primer 5′-CGGAGTCAACGGATTTGGTCGTAT-3′ and reverse primer 5′-AGCCTTCTCCATGGTGGTGAAGAC-3′. To examine the signal transduction pathway of MIF, human dermal fibroblasts were stimulated with or without MIF and various inhibitors of molecules involved in the signal transduction pathway for 24 h. Total RNA was isolated from monolayered cultures using an Isogen RNA extraction kit according to the manufacturer's protocols. RNA was quantified by spectrophotometry, and equal amounts of RNA (5–10 μg) from samples were loaded on a formaldehyde-agarose gel. The gel was stained with ethidium bromide to visualize the RNA standards, and the RNA was transferred onto a nylon membrane. Fragments obtained by restriction enzyme treatments for MMP-1, TIMP-1, GAPDH, and MIF were labeled with [α-^{32}P]dCTP using a DNA random primer labeling kit. Hybridization was carried out at 42 °C for 24 h. Post-hybridization washes were performed twice in 0.1% SDS, 0.2× SSC (1× SSC: 0.15 M NaCl, 0.015 M sodium citrate) at 65 °C for 15 min. The radioactive bands were visualized by autoradiography on Kodak X-AR5 film and quantitatively analyzed using the NIH Image system. Multiple autoradiographic data were examined to ensure that the results reflected those produced in the linear range of the film. The results were normalized by GAPDH mRNA levels. Comparison of ethidium bromide-stained gels with the corresponding GAPDH mRNA levels showed that GAPDH mRNA levels reflected the total RNA loaded onto the gels.

ELISA for MIF—To examine the concentration of MIF from cultured fibroblasts, supernatants from cultured fibroblasts by UVA were examined using an MIF ELISA system essentially as described previously (19). For this assay we used recombinant human MIF to obtain the standard curve, in which good linearity was demonstrated between MIF concentrations (1 to 200 ng/ml) and absorbency.

ELISA for MMP-1—After reaching confluence, the cells were trypsinized and then plated on a 24-well culture dish at 4 × 10^4 cells per well in 0.5 ml of DMEM containing 10% FCS. After 48 h, the medium was replaced with 0.5 ml of serum-free DMEM containing various doses of MIF (0, 0.1, 1, 10, and 100 ng/ml). After 24 h, the supernatants were collected and subjected to ELISA for MMP-1. The protein level values for MMP-1 were added to those of the supernatants. For the time-course study, we used a procedure similar to that used for the dose response study in the presence of 100 ng/ml MIF using human dermal fibroblasts. Aliquots were obtained at the indicated intervals for up to 48 h. MMP-1 was assayed by an ELISA using a Biotrack MMP-1 assay kit according to the manufacturer's protocol. The minimal sensitivity of the assay system was 6.25 ng/ml, and good linearity was observed at amounts up to 100 ng/ml. Using this ELISA system, all forms of MMP, including pro-MMP-1, MMP-1, and MMP-1 complexes with TIMP-1, could be measured.

Determination of MMP-1 Activity in Culture Media of Fibroblasts—Culture media of dermal fibroblasts were collected at the indicated intervals in the presence of MIF (100 ng/ml) for up to 48 h, and concentrated (10-fold) using Centriprep YM-30 (Millipore, Bedford, MA) for further analyses. Then, MMP-1 activities were determined by heparin-enhanced zymography as previously described (20). In brief, gelatin (0.5 mg/ml) was embedded in 7.5% SDS-PAGE gel. Samples (15 μg protein for each sample) were treated with sample buffer without dithiothreitol at room temperature and electrophoresed until the dye-

front was near the bottom of the gel. To produce the enhancing effects, 10 ml heparin (0.3 mg/ml in 1× sample buffer without SDS) was added to the lanes 20–30 min after electrophoresis began. Each gel was washed two times with 2.5% Triton X-100, 50 mM Tris, pH 7.5, 4 °C, 20 min each, to remove SDS and then two times with buffer plus 5 mM $CaCl_2$. The gel was washed three times with incubation buffer (50 mM Tris, pH 7.5, 5 mM $CaCl_2$) and then incubated in this buffer with added protease inhibitors (50 μM each of z-phe-chloromethylketone and tosyl-phe-chloromethylketone and aminoethyl benzenesulfonyl fluoride) for 18 h at 37 °C with gentle shaking. Gels were stained with 0.1% Coomassie Blue in 40% MeOH, 10% acetic acid, for 45 min, and destained with 7% acetic acid. A positive control for recombinant human MMP-1 was used to detect the molecules of MMP-1.

Western Blot Analysis—Cells (1×10^6 cells) were disrupted with a Polytron homogenizer (Kinematica, Lucerne, Switzerland). The protein concentrations of the cell homogenates were quantified using a Micro BCA protein assay reagent kit. Equal amounts of homogenates were dissolved in 20 μl of Tris-HCl, 50 mM (pH 6.8), containing 2-mercaptoethanol (1%), sodium dodecyl sulfate (SDS) (2%), glycerol (20%), and bromphenol blue (0.04%), and the samples were heated to 100 °C for 5 min. The samples were then subjected to SDS-PAGE and transferred electrophoretically onto a nitrocellulose membrane. The membranes were blocked with 1% nonfat dry milk in phosphate-buffered saline, probed with anti-phospho-Raf, or anti-phospho-MAPK antibody, then allowed to react with goat anti-rabbit IgG Ab coupled with horseradish peroxidase. The resultant complexes were processed for the detection system according to the manufacturer's protocol. To investigate the involvement of tyrosine kinase in PKC phosphorylation, cells were serum-starved for 24 h and challenged with MIF (100 ng/ml) 30 min after the addition of PP2 (10 μM), tyrosine kinase inhibitor (genistein) (100 μM), and Src family tyrosine kinase inhibitor (Herbimycin A) (10 μM) in serum-free medium. After 60 min, the cells were harvested and subjected to Western blot analysis for phosphorylation of phospho-PKCα/βII. To investigate the involvement of tyrosine kinase and PKC in the phosphorylation of MAPK by MIF, fibroblasts pretreated with inhibitors against tyrosine kinase and PKC for 30 min were stimulated by MIF for 60 min. Then cell lysates were prepared and subjected to Western blot analysis. For loading controls, we carried out Western blot analysis on β-actin using an anti-β-actin antibody.

Transfection of CSK and CSK⁻—At 24 h after plating the fibroblasts on 6-well dishes, plasmid DNAs of CSK and CSK⁻ were transfected using FuGENE 6 according to the manufacturer's protocol. For each dish, CSK or CSK⁻ plasmid (1 μg) was transfected to cultured cells in serum-free medium for 24 h. Following this, cells were stimulated with MIF (100 ng/ml) for 60 min. The cell lysates were prepared and subjected to Western blot analysis for phosphorylation of PKC and MAPK.

Electrophoretic Gel Mobility Shift Assay (EMSA)—Human dermal fibroblasts were incubated with 100 ng/ml MIF for the indicated times, and the nuclear proteins extracted. The consensus AP-1 oligonucleotide was annealed and labeled with digoxigenin-11-ddUTP. To prevent nonspecific binding, 0.1 μg of poly(d(I-C)) was added to the binding reaction. The mixture was transferred to a 6% polyacrylamide gel and submitted to gel electrophoresis. Following electrophoresis, the oligonucleotide-protein complexes were electroblotted to a Nylon membrane. The digoxigenin-labeled DNA oligonucleotides were visualized by an enzyme immunoassay using anti-digoxigenin-AP, Fab-fragments, and the chemiluminescent substrate CSPD, as described by the manufacturer (Roche Applied Science). The generated chemiluminescence was visualized on x-ray film.

Statistics—Values are expressed as means ± S.E. of the respective test or control group. Statistical significances between the control group and test groups were evaluated by the Student's *t* test. Data are representative of at least three experiments.

RESULTS

MIF Production in Response to UVA Irradiation in Human Dermal Fibroblasts—We first examined whether UVA is able to stimulate production of MIF in dermal fibroblasts. Fibroblasts were stimulated by UVA, and it was found that UVA up-regulates MIF production in a dose-dependent manner (Fig. 1). After 24-hr UVA stimulation at an intensity of 20 J/cm², the MIF content was remarkably elevated, showing a more than 8-fold increase compared with levels in the absence of UVA stimulation.

Effects of MIF on MMP-1 and TIMP-1 mRNA Expression—In human dermal fibroblasts, MMP-1 mRNA was up-regulated in

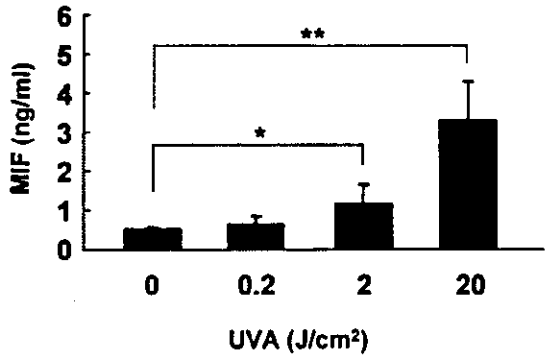

FIG. 1. **Induction of MIF in human fibroblasts by UVA radiation.** Fibroblasts were treated with UVA radiation and cultured for 24 h. MIF in the culture media was measured by ELISA, as described under "Experimental Procedures." The values are the mean ± S.E. of three different experiments. **, $p < 0.01$ and *, $p < 0.05$ for 20 J/cm² *versus* 0 J/cm².

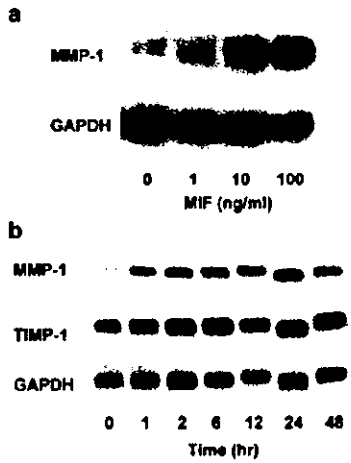

FIG. 2. **Effects of MIF on MMP-1 mRNA expression in dermal fibroblasts.** Total RNAs extracted from dermal fibroblasts were treated with various concentrations of MIF in serum-free medium at the indicated intervals. Northern blot analysis was carried out as described under "Experimental Procedures." The membranes were hybridized with radiolabeled cDNA probes of MMP-1 and GAPDH and then visualized by autoradiography. *a*, the dose-dependent expression of MMP-1 mRNA expression in response to MIF ranging from 0 to 100 ng/ml after 24 h-MIF stimulation. *b*, time-dependent expression of MMP-1 mRNA in response to MIF (100 ng/ml).

a dose-dependent manner in response to MIF, ranging from 1 ng/ml to 100 ng/ml for per 24-hr treatment (Fig. 2*a*). A time-course study of MMP-1 and TIMP-1 in dermal fibroblasts was then performed. MMP-1 mRNA expression increased in response to MIF (100 ng/ml) at 1 h post stimulation and reached a maximum at 24 h (Fig. 2*b*). MIF mRNA levels were slightly down-regulated at 48 h. TIMP-1 mRNA was also elevated, but the increase was less significant than MMP-1 mRNA, although the levels were sustained for at least 48 h.

MMP-1 Production and Activation in Response to MIF—MMP-1 protein was detected in the culture supernatant of human dermal fibroblasts. In a dose-response study, the MMP-1 protein levels were significantly up-regulated at doses of 100 ng/ml (Fig. 3*a*). For the time-course study, MMP-1 in the supernatant was elevated at 12 h after MIF stimulation (100 ng/ml), reached a maximum at 24 h, and was sustained for at least 48 h (Fig. 3*b*). To investigate MIF induced MMP-1 activity, zymography was performed. We used heparin to enhance the signal, because MMP-1 is difficult to detect at low levels in

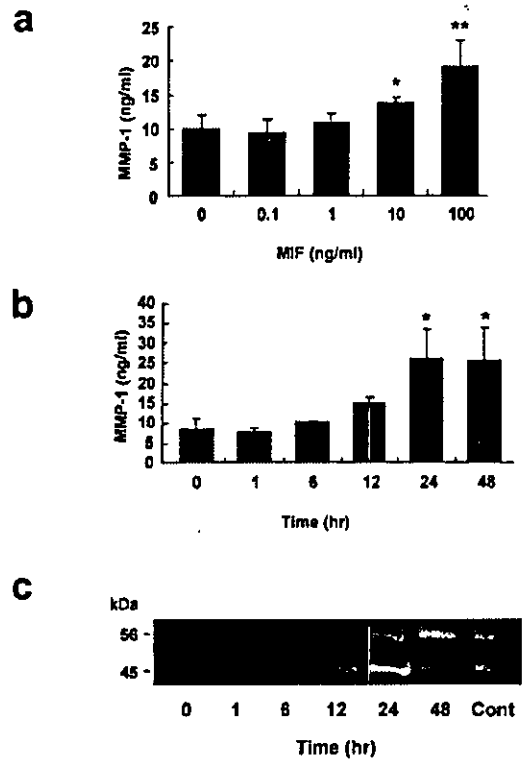

FIG. 3. **Effects of MIF on the production and activation of MMP-1 in dermal fibroblasts.** *a*, aliquots of the culture supernatants of dermal fibroblasts in serum-free medium were collected after treatment with various concentrations of MIF for 24 h, then subjected to ELISA for MMP-1 ($n = 5$). **, $p < 0.01$ and *, $p < 0.05$ *versus* control (0 ng/ml). *b*, culture supernatants of dermal fibroblasts were collected at the indicated times in the presence of 100 ng/ml MIF for up to 48 h and then subjected to ELISA on MMP-1 ($n = 5$), *, $p < 0.05$ *versus* control (0 h). *c*, culture supernatants of dermal fibroblasts were collected at the indicated times in the presence of 100 ng/ml MIF for up to 48 h. The supernatants were concentrated 10-fold and subjected to heparin-enhanced zymography. Molecular weight markers at 56 and 45 kDa show latent and active forms of MMP-1, respectively. *Cont*, stimulation with recombinant MMP-1 for 48 h.

conventional gelatin zymography (20). MMP-1 in the active form (45 kDa) in fibroblasts was enhanced by 100 ng/ml MIF stimulation, reached a maximum at 24 h, and slightly decreased at 48 h (Fig. 3*c*).

Inhibition of MMP-1 Production of Dermal Fibroblasts by a Neutralizing anti-MIF Antibody—We attempted to determine whether neutralizing anti-MIF antibody influences UVA-induced MMP-1 expression in human dermal fibroblasts. By Northern blot analysis, we found that the anti-MIF antibody (1 and 10 μg/ml) significantly down-regulated the expression of MMP-1 mRNA induced by UVA stimulation (20 J/cm^2) (Fig. 4*a*). Based on the results of the Western blot analysis, we confirmed that MMP-1 production is inhibited by the anti-MIF antibody (Fig. 4*b*).

UVA-induced MMP-13 Production in Cultured Dermal Fibroblasts and Skin Tissue in Vivo from MIF-deficient Mice—To clarify whether synthesis of MIF is required for the UVA-induced collagenase, we used dermal fibroblasts from MIF-deficient mice in the production of mouse collagenase MMP-13. Although MMP-13 plays a restricted role in human tissues, it is the predominant tissue collagenase in rodents. Twenty-four hours after UVA irradiation, a significant decrease in viability was observed only after more than 15 J/cm^2 UVA irradiation in fibroblasts from MIF-deficient mouse (data not shown); we therefore used up to 10 J/cm^2 UVA irradiation for experiment.

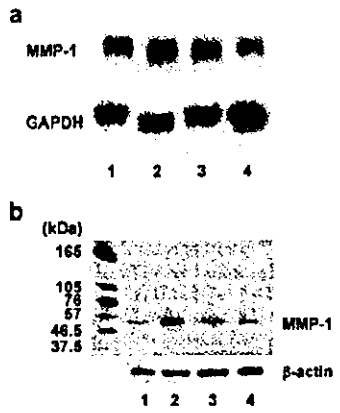

FIG. 4. **Effects of anti-MIF antibody on the UVA-induced MMP-1 mRNA.** *a*, fibroblasts were irradiated (UVA 20 J/cm^2) in the presence of an anti-MIF antibody (1 and 10 μg/ml) in DMEM supplemented with 10% FCS and then further incubated for 24 h. Expression of MMP-1 mRNA was assessed by Northern blot analysis. *Lane 1*, untreated dermal fibroblasts; *lane 2*, fibroblasts stimulated by UVA; *lane 3*, UVA-stimulated fibroblasts with the anti-MIF antibody (1 μg/ml); *lane 4*, UVA-stimulated fibroblasts with the anti-MIF antibody (10 μg/ml). *b*, cell lysates (40 μg) of 20 J/cm^2 UVA-stimulated fibroblasts with anti-MIF antibodies (1 and 10 μg/ml) cultured for 24 h were subjected to Western blot analysis using an anti-MIF antibody. The results with anti-β-actin antibody are shown as a control. *Lane 1*, untreated dermal fibroblasts; *lane 2*, fibroblasts stimulated by UVA; *lane 3*, UVA-stimulated fibroblasts with the anti-MIF antibody (1 μg/ml); *lane 4*, UVA-stimulated fibroblasts with the anti-MIF antibody (10 μg/ml).

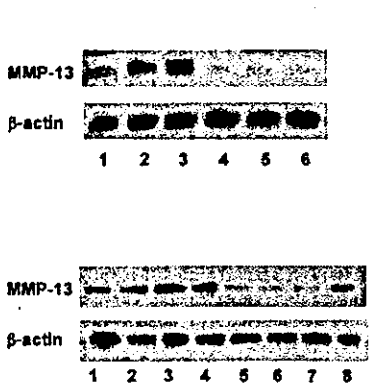

FIG. 5. **UVA-induced MMP-13 production from cultured dermal fibroblasts and skin tissues of MIF-deficient mice.** *a*, cultured 3rd passage dermal fibroblasts from MIF-deficient mice or BALB/c WT mice were irradiated with UVA at 0, 5, 10 J/cm^2. After 24 h, cell lysates (40 μg) were subjected to Western blot using anti-MMP-13 antibody. The results with anti-β-actin antibody are shown as a control. *Lane 1*, WT mouse, 0 J/cm^2; *lane 2*, WT mouse, 5 J/cm^2; *lane 3*, WT mouse, 10 J/cm^2; *lane 4*, MIF-deficient mouse, 0 J/cm^2; *lane 5*, MIF-deficient mouse, 5 J/cm^2; *lane 6*, MIF-deficient mouse 10 J/cm^2. *b*, shaved abdomens of MIF-deficient mice or BALB/c WT mice were irradiated with UVA at 0, 10, 20, and 30 J/cm^2. After 24 h, skin homogenates were subjected to Western blotting using an anti-MMP-13 antibody. *Lane 1*, WT mouse with 0 J/cm^2; *lane 2*, WT mouse with 10 J/cm^2; *lane 3*, WT mouse with 20 J/cm^2; *lane 4*, WT mouse with 30 J/cm^2; *lane 5*, MIF-deficient mouse with 0 J/cm^2; *lane 6*, MIF-deficient mouse with 10 J/cm^2; *lane 7*, MIF-deficient mouse with 20 J/cm^2; *lane 8*, MIF-deficient mouse with 30 J/cm^2.

After 24 h of UVA irradiation (0–10 J/cm^2), elevated MMP-13 production was observed in cell lysates of dermal fibroblasts in control WT mice in a dose-dependent manner (Fig. 5*a*). On the other hand, UVA irradiation appeared to have no effect on MMP-13 production in dermal fibroblasts of MIF-deficient mice. Consistent with these results *in vitro*, elevated MMP-13 production was also observed in the skin of control WT mice in

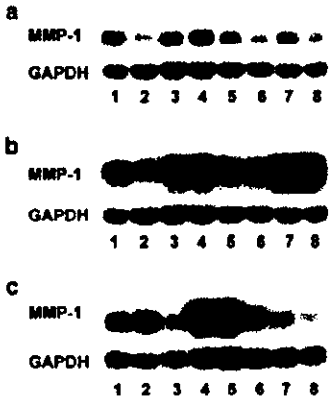

FIG. 6. **Effects of reagents on MIF-induced MMP-1 mRNA expression.** Dermal fibroblasts were preincubated for 30 min with various concentrations of inhibitors prior to challenge with MIF. The cells were then incubated for 24 h in the presence or absence of inhibitors and visualized by autography. *a*, tyrosine kinase inhibitor genistein and Src family tyrosine kinase inhibitor herbimycin A; *lane 1*, no stimulation; *lane 2*, genistein 100 μM; *lane 3*, herbimycin A 10 μM; *lane 4*, MIF 100 ng/ml; *lane 5*, MIF 100 ng/ml + genistein 10 μM; *lane 6*, MIF 100 ng/ml + genistein 100 μM; *lane 7*, MIF 100 ng/ml + herbimycin A 1 μM; *lane 8*, MIF 100 ng/ml + herbimycin A 10 μM. *b*, MEK inhibitor PD98089 and p38 inhibitor SB203580; *lane 1*, no stimulation; *lane 2*, PD98059 40 μM; *lane 3*, SB203580 10 μM; *lane 4*, MIF 100 ng/ml; *lane 5*, MIF 100 ng/ml + PD98059 10 μM; *lane 6*, MIF 100 ng/ml + PD98059 40 μM; *lane 7*, MIF 100 ng/ml + SB203580 5 μM; *lane 8*, MIF 100 ng/ml + SB203580 10 μM. *c*, PKA inhibitor H89 and PKC inhibitor GF109203X. *Lane 1*, no stimulation; *lane 2*, H89 10 μM; *lane 3*, GF109203X 10 μM; *lane 4*, MIF 100 ng/ml; *lane 5*, MIF 100 ng/ml + H89 1 μM; *lane 6*, MIF 100 ng/ml + H89 10 μM; *lane 7*, MIF 100 ng/ml + GF109203X 1 μM; *lane 8*, MIF 100 ng/ml + GF109203X 10 μM.

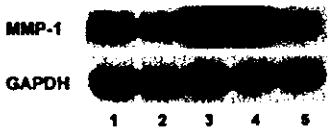

FIG. 7. **Effects of JNK inhibitor on MIF-induced MMP-1 mRNA expression.** Dermal fibroblasts were preincubated for 30 min with various concentrations of inhibitors prior to challenge with MIF similar to the procedure in Fig. 6. The cells were then incubated for 24 h in the presence or absence of JNK inhibitor SP600125. *Lane 1*, no stimulation; *lane 2*, SP600125 30 μM; *lane 3*, MIF 100 ng/ml; *lane 4*, MIF 100 ng/ml + SP600125 3 μM; *lane 5*, MIF 100 ng/ml + SP600125 30 μM.

a dose-dependent manner after UV irradiation *in vivo*, whereas UVA irradiation had little effect on MMP-13 production in the skin of MIF-deficient mice (Fig. 5*b*).

Effects of Inhibitors on MMP-1 Expression in Response to MIF—To examine the signal transduction pathway of MIF, we examined the effects of several inhibitors of molecules involved in the signal transduction pathway when dermal fibroblasts were stimulated with MIF relevant to MMP-1 up-regulation. Several inhibitors were tested, including tyrosine kinase inhibitors genistein and herbimycin A, PKA inhibitor H89, PKC inhibitor GF109203X, and MEK inhibitor PD98089. We found that these inhibitors for tyrosine kinase, PKA, PKC, and MEK inhibitors significantly reduced MMP-1 mRNA stimulated by MIF (Fig. 6, *a–c*). In contrast, the SB203580 (p38 inhibitor) failed to inhibit the up-regulation of MMP-1 mRNA (Fig. 6*b*). Furthermore, we found that JNK inhibitor SP600125 also significantly suppressed MMP-1 mRNA stimulated by MIF (Fig. 7).

Phosphorylation of PKC, Raf, and MAPK—We investigated the phosphorylation of PKC, Raf, and MAPK after MIF stimulation in dermal fibroblasts. The phosphorylation of PKC pan, PKCα/βII, PKCδ (Thr^{505}) and PKCδ (Ser^{643}) reached a maximum level at 30 min in response to MIF, and was down-regulated after 120 min, whereas PKCζ/λ (Thr$^{410/403}$) was not phosphorylated (Fig. 8). Other PKC isoforms, including PKD/PKCμ (Ser$^{744/748}$), PKD/PKCμ (Ser^{916}), and PKCθ (Thr^{538}), were not phosphorylated (data not shown). The phosphorylation of Raf reached a maximum level at 15 min, and that of MAPK was at a maximum level at 60 min (Fig. 9).

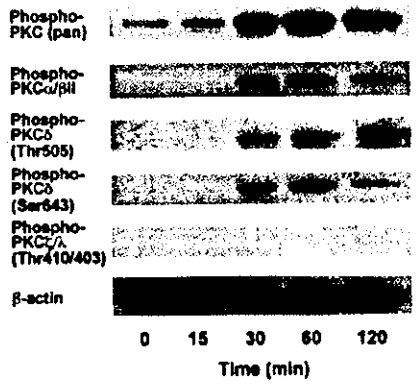

FIG. 8. **Phosphorylation of PKC in response to MIF.** Dermal fibroblasts were stimulated for the indicated time intervals (0–120 min) by MIF (100 ng/ml). Western blot analysis was performed on whole cell lysates (40 μg) and antibodies against phospho-PKCpan, PKCα/βII, PKCδ (Thr^{505}), PKCδ (Ser^{643}), and PKCζ/λ (Thr$^{410/403}$) were used. After removal of the original signals, we carried out Western blot analysis of β-actin on the same membranes as loading controls for each PKC isoform as described under "Experimental Procedures." Since the patterns of protein bands of β-actin for all 5 isoforms were similarly detected, we present the results of β-actin on phospho-PKC(pan) as a representative at the *bottom* of the lanes.

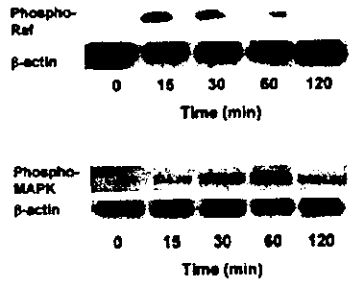

FIG. 9. **Phosphorylation of Raf and MAPK in response to MIF.** Dermal fibroblasts were stimulated for the indicated time intervals (0–120 min) by MIF (100 ng/ml). Western blot analysis was performed on whole cell lysates (40 μg) and antibodies against phospho-Raf, and anti-phospho-p44/p42-MAPK were used. Western blot analysis for β-actin is shown as a control.

Effects of Protein Kinase Inhibitors on PKC and MAPK Activation by MIF—To assess the involvement of tyrosine kinase on PKC and MAPK activation in dermal fibroblasts, we examined whether these inhibitors suppressed the phosphorylation of PKCα/βII and MAPK in response to MIF (100 ng/ml) at 60 min. tyrosine kinase inhibitors, including PP2, genistein, and herbimycin A, were found to suppress PKCα/βII phosphorylation induced by MIF (Fig. 10*a*). Furthermore, we demonstrated that genistein, herbimycin A and PKC inhibitor GF109203X suppressed the phosphorylation of MAPK (Fig. 10*b*).

Effects of CSK on MIF-induced Phosphorylation of PKC and MAPK—Among nonreceptor tyrosine kinases, Src family tyrosine kinases have been reported to activate MAPK (21). We examined the role of Src family tyrosine kinases in MIF-induced phosphorylation of PKC and MAPK using a negative regulator, CSK. We transfected a CSK gene-containing plasmid into cultured dermal fibroblasts and examined the phosphoryl-